RESEARCH REPORT

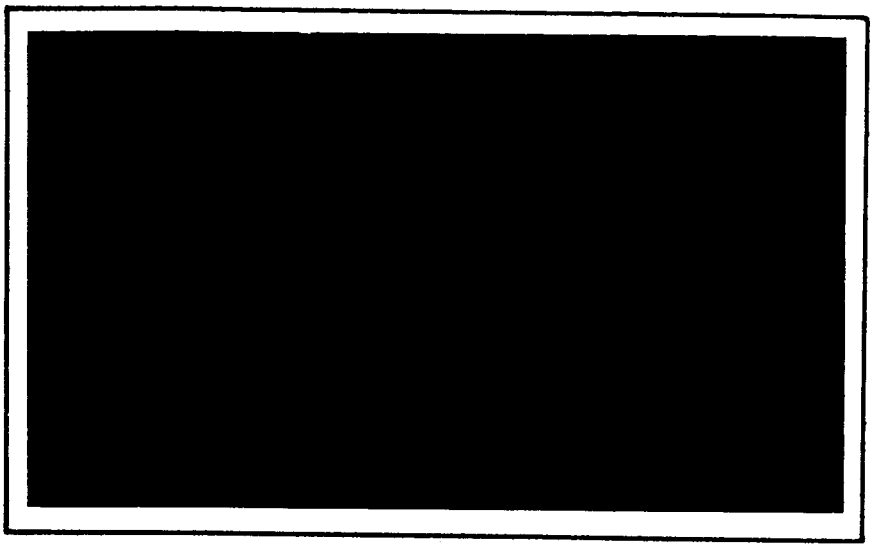

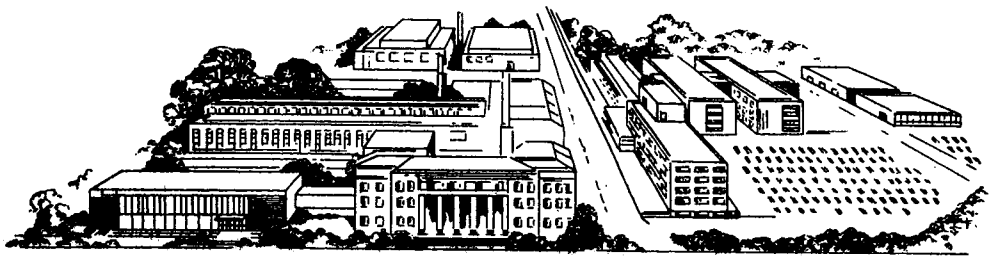

BATTELLE

MEMORIAL INSTITUTE

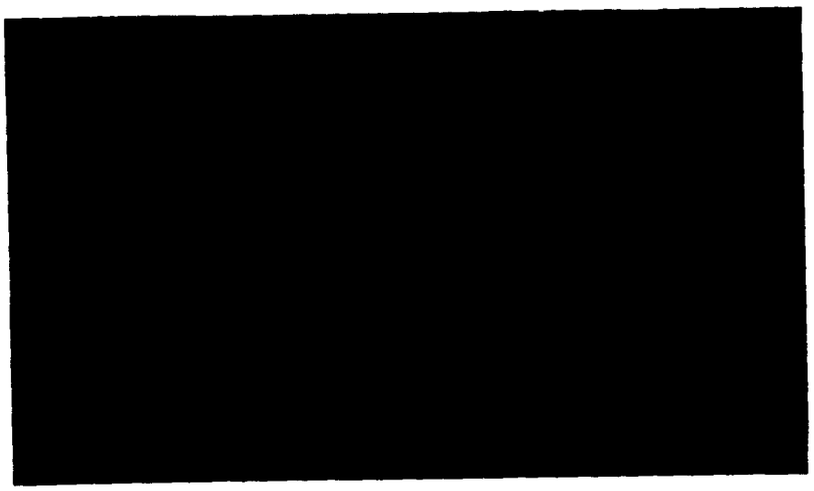

BATTELLE FIELDS OF RESEARCH

Aeronautics—Astronautics
Agricultural Chemistry
Agricultural Economics
Alloy Development
Applied Mathematics
Area Economics
Biochemistry
Biophysics—Bionics
Catalysis—Surface Chemistry
Ceramics
Chemical Engineering
Chemical Processes
Communications Science
Computer Technology
Corrosion Technology
Earth — Atmospheric Sciences
Electrochemistry
Electronics
Energy Conversion
Engineering—Structural Materials
Environmental Systems
Extractive Metallurgy
Extreme-Temperature Technology
Ferrous Metallurgy
Food Technology
Foundry Practice
Fuels—Combustion
Glass Technology
Graphic Arts Technology
Immunology—Cancer Studies
Industrial Economics
Industrial Physics
Information Research
Inorganic Chemistry
Instrumentation
Light Alloys—Rare Metals
Lubricant Technology
Materials Separation—Concentration
Mechanical Engineering
Metal Fabrication Engineering
Metal Finishing
Metallurgical Processes
Microbiology
Microscopy—Mineralogy
Nondestructive-Evaluation Technology
Nonferrous Metallurgy
Nucleonics
Organic Chemistry
Organic Coatings
Packaging Research
Particle Dynamics
Petrochemicals
Petroleum Engineering
Pharmaceutical Chemistry
Physical Chemistry
Product Development
Production Engineering
Psychological Sciences
Pulp—Paper Technology
Radioisotopes—Radiation
Reactor Technology
Refractories
Reliability Engineering
Rubber—Plastics
Semiconductors—Solid-State Devices
Sound — Vibration
Systems Engineering
Textiles—Fibers
Theoretical—Applied Mechanics
Thermodynamics
Transportation
Welding—Metals-Joining Technology
Wood—Forest Products

SECOND QUARTERLY PROGRESS REPORT

on

DEVELOPMENT OF IMPROVED THERMOELECTRIC MATERIALS FOR SPACECRAFT APPLICATIONS

to

GEORGE C. MARSHALL
SPACE FLIGHT CENTER
NATIONAL AERONAUTICS AND
SPACE ADMINISTRATION

January 29, 1965

Contract No. NAS8-11452
Control No. DCN 1-4-50-01159-01 & S1 (1F)
CPB 02-1200-64

For the Period
October 1, 1964, to January 1, 1965

by

E. P. Stambaugh, L. K. Matson, B. G. Koehl,
R. Simon, and E. H. Lougher

BATTELLE MEMORIAL INSTITUTE
505 King Avenue
Columbus, Ohio 43201

(1) Theoretical Study

(2) Experimental Study (Thermoelectric Cooling)

(a) Preparation and Evaluation of Ag $(Fe, Sb)_x$ $(Se, Te)_y$ Ternaries

(b) Preparation and Evaluation of $AgSb_kFe_\ell Se_mTe_n$ Alloys

(c) Preparation and Evaluation of n-p Couples of Promising Alloy(s)

(d) Optimization of n- and p-Type Bi-Sb Alloys for Low-Temperature Cooling

(3) Final Report (Preparation, Submission, and Approval)

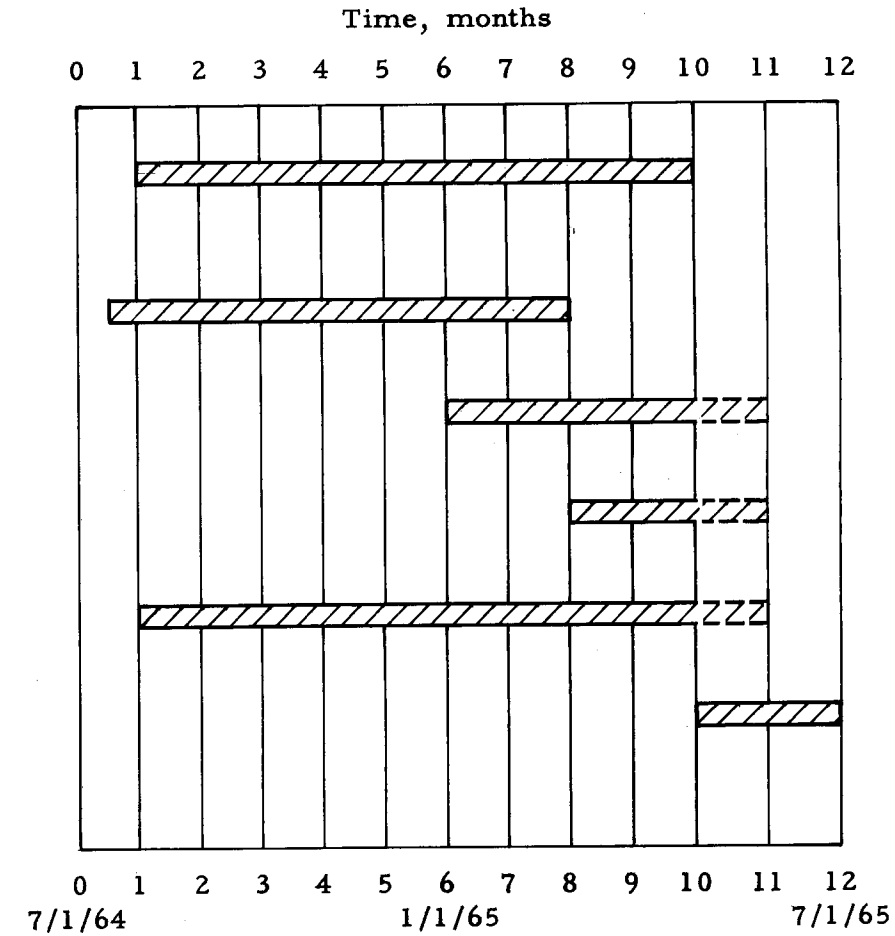

PROGRAM-PLANNING CHART

TABLE OF CONTENTS

LIST OF TABLES

LIST OF FIGURES

LIST OF FIGURES
(Continued)

DEVELOPMENT OF IMPROVED THERMOELECTRIC MATERIALS FOR SPACECRAFT APPLICATIONS

by

E. P. Stambaugh, L. K. Matson, B. G. Koehl,
R. Simon, and E. H. Lougher

INTRODUCTION

This is the Second Quarterly Progress Report on the project, "Development of Improved Thermoelectric Materials for Spacecraft Applications", covering the period from October 1, 1964, to January 1, 1965. The program, outlined in PR DCN 1-4-50-01159-01 & S1 and in Battelle's proposal dated June 4, 1964, is being carried out under Contract NAS8-11452. This work is a continuation of that conducted by Ohio Semiconductors Division, Tecumseh Products Company, under Contract NAS8-11075.

The objective of this research is the study and optimization of selected materials for use in thermoelectric cooling in a space environment. The materials to be investigated are Bi-Sb alloys and alloys in the Ag-Sb-Fe-Te-Se system.

ABSTRACT

During this period, experimental effort was directed toward optimization of n- and p-type Bi-Sb alloys for low-temperature thermoelectric cooling and toward the preparation and evaluation of $Ag(Fe, Sb)_x(Se, Te)_y$ ternaries for use at higher temperatures. Theoretical work was devoted to extension of calculations of the thermoelectric figure of merit of various materials based on the two-energy-band model and to examination of the results.

Analytical techniques based on $\sigma_o e^r$ and Z(max)T values for screening and evaluating materials for potential thermoelectric applications are discussed. The quantity $\sigma_o e^r$ which can be obtained from the resistivity and Seebeck coefficient values and which is a characteristic constant of a material is directly indicative of the quality of the electronic transport properties of a single-band material pertinent to its potentialities as a thermoelectric material. It has been established that a value of $\sigma_o e^r$ of much less than 500 $ohm^{-1}\text{-}cm^{-1}$ is sufficient criterion for rejecting a material without need for further measurements, if the material is known to be essentially extrinsic and to have a single conduction band. If not, the indicated value serves as a rough acceptance guide. If a material has an acceptable $\sigma_o e^r$ value, a good estimate of Z(max)T can be obtained from Seebeck coefficient, resistivity, and thermal conductivity by plotting the experimental point (S, $K\rho/T$) on a graph of $K/\sigma T \times 10^8 V/(°K)^2$ versus $S\mu V/°K$.

Continued study of the Ag-Sb-Te system has indicated that the region of single-phase material exists near the $Ag_{22}Sb_{27}Te_{52}$* composition and promising thermoelectric properties are exhibited by near single-phase alloys of approximately that composition;

*Subscripts are atomic percentages.

σ_o values greater than 500 ohm^{-1}-cm^{-1} were obtained. In these alloys, the Seebeck coefficient is rather insensitive to small changes in composition and/or the presence of small amounts of minor phases (at least, at temperatures above 200°K), whereas, the resistivity is very sensitive to such changes. Results suggest that other factors such as crystallinity, homogeneity, doping, etc., also may affect the thermoelectric properties of the alloy.

Considerable improvement in the thermoelectric properties of $AgSbSe_2$ was attained by doping with 0.01 atomic percent silver. However, the σ_o value of the doped specimen was still very low (90 ohm^{-1}-cm^{-1}).

$AgFeTe_2$ and $AgFeSe_2$ ingots prepared by several methods were examined and found to be polyphase.

Several n-type (tellurium-doped and undoped) and p-type (tin-doped) $Bi_{86}Sb_{14}$ alloy ingots were prepared and evaluated. Reducing the tin content of the alloy from 3.4 atomic percent to 1.9 atomic percent (nominal compositions) improved the thermoelectric properties of the p-type alloy slightly. Seebeck-coefficient values of the tellurium-doped alloy (n-type) were very low, indicating that it was overdoped for thermoelectric use.

Calculations of the figure of merit of thermoelectric materials based on the two-energy-band model are extended to cover wider ranges of values of the parameters of this model. The results of these computations in conjunction with consideration of the temperature dependencies of the model parameters enable estimations to be made of the value of $(ZT)_{max}$ for various materials. The parameter $(ZT)_{max}$ is the maximum dimensionless thermoelectric figure of merit as optimized both with respect to impurity doping and with respect to temperature; it is the quantity of significance in evaluating potential thermoelectric materials.

Consideration of the temperature variation of Z(max)T, the figure of merit as optimized with respect to impurity doping only, has resulted in the discovery of another possible reason for the difficulty in finding higher $(ZT)_{max}$ materials: The greater the value of $(ZT)_{max}$, the narrower is the range of temperature over which $ZT \approx (ZT)_{max}$. Another reason previously known but confirmed by the additional computations is that materials with higher values of the material parameter must also have either larger band gaps or greater degrees of asymmetry in the σ_o values for electrons and holes in order to realize the full benefits of the improved material parameter. The quantity σ_o is the measure of the electronic transport contribution to the material parameter.

The values of the two-band-model parameters are computed and tabulated for the common elemental and binary compound semiconductors for which the necessary data were found in the literature. Some preliminary observations made from these tabulations seem to confirm the theoretical expectation that high σ_o values are associated with multivalley band structures with a high degree of mass anisotropy per valley. The degree of overall anisotropy of electrical conductivity in the crystal seems to be of little consequence, nor have we found any evident correlation with the type of crystal structure or chemical binding. There is also a poor correlation between σ_o and the value of the charge carrier mobility, even within a group of similar compounds. The thermoelectric properties of a Ge-Si alloy are also shown to be superior to those of a Bi_2Te_3-Bi_2Se_3 alloy, each in its own temperature range. The possible uniqueness of the particular crystal structure, energy-band structure, or chemical bonding of the latter from the viewpoint of superiority of thermoelectric properties is questionable.

WORK PREVIOUSLY ACCOMPLISHED

During the first quarter of this contract period, experimental effort was devoted to the preparation and evaluation of $Bi_{86}Sb_{14}$ alloys (n- and p-type) and single-phase ternaries in the $Ag(Fe,Sb)_x(Se,Te)_y$ system. Theoretical effort was devoted to correlation of the ionicity concept with the theory of the fundamental semiconductor characteristics that determine thermoelectric performance.

Large single crystals of n- and p-type Bi-Sb alloys were prepared by zone levelling at a crystallization rate of 3.2 cm per hour. An n-type, undoped specimen containing 14.6 atomic percent antimony was found to have a figure of merit of $3.79 \times 10^{-3}/°K$ at 80°K. Measurements on the p-type (tin doped) alloy were conducted during the second quarter.

Single phase $AgSbSe_2$ was prepared by the furnace cool-anneal method. A specimen from this ingot had Seebeck-coefficient and resistivity values at 300°K of 450 $\mu V/°K$ and 3.0 ohm-cm, respectively. The temperature dependence of these parameters indicated that the specimen probably was intrinsic. Doping studies conducted during the second period and discussed in this report were made to determine the capability of this material for thermoelectric-cooling applications. The other ternaries, $AgSbTe_2$, $AgFeTe_2$, and $AgFeSe_2$, prepared by the furnace cool-anneal method, were polyphase. The $AgSbTe_2$ contained only a minor second phase, whereas the $AgFeSe_2$ and $AgFeTe_2$ each contained two phases of comparable concentrations. Other methods of preparation (quench-anneal and zone levelling-zone refining) were used in an effort to prepare each of these latter ternaries as single-phase materials. Results are discussed in this report.

The relationship between the pertinent dimensionless energy-band structure and scattering parameters and the maximum figure of merit that can be attained by impurity doping of an essentially single-band material was reviewed. Suchet's ionicity-parameter criteria for selecting potential thermoelectric materials were examined in light of these relationships. It was tentatively concluded that these criteria are not likely to be useful for material selection. This tentative conclusion remains to be verified or modified on the basis of correlations between the results of the band-structure and ionicity criteria when applied to materials with known thermoelectric properties.

WORK ACCOMPLISHED DURING THIS PERIOD

During this period, experimental and theoretical studies were continued on the development of improved thermoelectric materials for spacecraft applications. Experimental effort was directed toward evaluating the ternaries, $AgSbTe_2$, $AgSbSe_2$, $AgFeTe_2$ and $AgFeSe_2$, and the Bi-Sb alloy system. Theoretical studies were concerned with examination of the band-theory dimensionless parameters for materials with various crystal structures, energy-band structures, and types of chemical bonding.

Experimental Investigation

Evaluation of Materials

In previous theoretical studies at Battelle, analytical techniques[1, 2]* have been developed for the evaluation and screening of materials for potential thermoelectric applications. Screening of materials is based on the quantity $\sigma_o e^r$ whereas evaluation is based on the value of $Z_{(max)}T$.

As discussed in the theoretical section of this report, the quantity $\sigma_o e^r$ is a valid measure of the quality of the charge-carrier-transport contribution to the thermoelectric figure of merit. The value of $\sigma_o e^r$ can be readily determined for extrinsic materials from the resistivity and Seebeck coefficient values using the procedure outlined in the First Progress Report. Consequently, it has been used previously at Battelle as a convenient criterion for the rapid screening of materials. Materials that are adjudged to be acceptable under the $\sigma_o e^r$ criterion are candidates for further testing to ascertain their thermoelectric potentialities.

The value of $\sigma_o e^r$ used as a dividing line between qualified acceptance and rejection of materials is somewhat arbitrary. The better thermoelectric materials seem to have $\sigma_o e^r$ values in the neighborhood of 10^3 ohm^{-1}-cm^{-1}. The room-temperature values of $\sigma_o e^r$ for room-temperature nBi_2Te_3 and pBi_2Te_3 are 1600 and 1200 ohm^{-1}-cm^{-1}, respectively.[3] The room-temperature $\sigma_o e^r$ of the $(Bi_2Te_3)_{90}$ $(Bi_2Se_3)_{10}$ alloy discussed above is 1400 ohm^{-1}-cm^{-1}. The $Ge_{70}Si_{30}$ alloy has a room-temperature $\sigma_o e^r$ value of 1200 ohm^{-1}-cm^{-1}. Fortunately, from the viewpoint of selecting materials for $(ZT)_{max}$ as well as for Z(max)T at a given temperature, the value of $\sigma_o e^r$ is not too temperature sensitive. (As discussed later, σ_o would be independent of temperature if m_d were temperature independent and μ varied strictly as $T^{-3/2}$.) The values of $\sigma_o e^r$ of nBi_2Te_3 and pBi_2Te_3 at T = 150°K are about 1500 and 1400 ohm^{-1}-cm^{-1}, respectively. $\sigma_o e^r$ of $nGe_{30}Si_{70}$ at 1100°K is 1400 ohm^{-1}-cm^{-1}.

In order to ensure that no material of potential thermoelectric importance would be inadvertently missed in a material survey, the threshold value of $\sigma_o e^r$ for further evaluation has been set at about 500 ohm^{-1}-cm^{-1}. A material with a σ_o value of 500 ohm^{-1}-cm^{-1} would have to have a K_L value of about 0.005 watt/cm°C in order to begin to be of thermoelectric interest (β = 0.22 at room temperature). The value of 500 ohm^{-1}-cm^{-1} for $\sigma_o e^r$ is based on the material being extrinsic and having single-band conduction. If the material is not known to be single band and extrinsic, the indicated $\sigma_o e^r$ values serve as a rough acceptance criterion for further consideration rather than as a good rejection criterion.

If further consideration is indicated from the $\sigma_o e^r$ values, then a good estimate of the maximum figure of merit of the material, Z(max)T with respect to impurity doping can be obtained from the Seebeck coefficient (S), resistivity (ρ), and thermal conductivity (K) values on a single specimen. This is done by plotting the experimental point $(S, K\rho/T)$ on a graph of $K/\sigma T$ versus S [see Reference (1)]. The position of the point on this characteristic curve also indicates whether the measured specimen is underdoped, overdoped, or about optimally doped. This analysis is for materials with a single-band conduction. However, it has been extended to include the two-band (electrons and holes) case.[2] As the impurity doping is changed, it is observed that a plot

*References are listed on page 50.

of S versus $K\rho/T$ is a closed-loop curve with two maxima of $ZT = S^2/(K\rho/T)$ along this curve, one for negative Seebeck coefficient and one for positive Seebeck coefficient. Thus measured values of S and $K\rho/T$ for only a few differently doped specimens are, in principle, sufficient to outline the characteristic curve for a given material, and hence, to determine the values of the pertinent dimensionless parameters and also the two values of Z(max)T.

Ternary Compounds

During this period, efforts were continued toward the preparation and evaluation of single-phase specimens of selected ternary compounds in the Ag-Sb-Fe-Te-Se system. Data on single-phase specimens of these materials are needed for guidance in development of the more complex alloys derived by partial substitution of iron and selenium in the Ag-Sb-Te lattice.

$AgFeSe_2$ and $AgFeTe_2$. Preparation. Both ternaries have now been prepared by furnace cool-anneal, by zone levelling-zone refining, and/or by quench-anneal methods. Each method of preparation is described in detail in the First Quarterly Progress Report. Conditions under which the preparations were conducted also are shown in the First Quarterly Progress Report and in Tables 1 and 2 of this report.

TABLE 1. CONDITIONS OF PREPARATION OF TERNARIES BY ZONE LEVELLING-ZONE REFINING

Ingot	Nominal Composition	Reaction Conditions		Zoning Conditions[a]			
		Temp, °C	Time, hr	Ambient Temp, °C	Zone Temp, °C	No. of Zone-Levelling Passes	No. of Zone-Refining Passes
21561-37	$AgFeTe_2$	535	15	605	800	4	11
		730	45				
21561-49[b]	$AgFeSe_2$	540	20	675	800	4	8
		665	48	650	≈825	0	6
		750	5				
21561-16	$AgSbTe_2$	500	3	500	600	4	12
		650	46				
		720	90				

(a) The zone-travel rate for both zone levelling and zone refining was 3.2 cm per hour.

(b) During the zoning operation, some material in the boat inadvertently transferred from the boat into one end of the reaction tube by vapor transport.

Homogeneity. The $AgFeTe_2$ and $AgFeSe_2$ ingots prepared by all three methods have been polyphase. Those prepared by furnace cool-anneal and quench-anneal contained two phases of approximately equal concentration and a minor third phase. In ingots prepared by zone levelling-zone refining, one phase predominated at one end of the ingot and the other phase predominated at the other. The first half of the $AgFeTe_2$ ingot (No. 21561-37) also contained a trace (less than 5 percent) of a third phase. Chemical analysis of a specimen from near the tail (last to freeze) end of this ingot showed the composition to be $Ag_{4.7}FeTe_{4.3}$. This can be rewritten in the form

$(Ag_{4.7}Te_{2.3})(FeTe_2)$ or, approximately, $(2.3\ Ag_2Te)(FeTe_2)$, suggesting that the phases present may have been predominantly Ag_2Te and $FeTe_2$. The melting point of the specimen, as determined by thermal analysis, was lower than those of the above binary compounds, but the difference could conceivably be due to eutectic formation.

TABLE 2. CONDITIONS OF PREPARATION OF SOME TERNARIES

Ingot	Composition	Reaction Conditions		Annealing Conditions		Method
		Temp,[a] °C	Time, hr	Temp, °C	Time, hr	
21561-60	$AgFeTe_2$	850	63	649	52	Q-A[b]
21561-4	$AgFeTe_2$	742	22	500	22	FC-A[c]
21561-64	$Ag_{24}Sb_{29}Te_{47}$	693	40	500	42	Q-A
21561-63	$Ag_{22}Sb_{27}Te_{51}$	693	40	500	42	Q-A
21561-79	$Ag_{21.6}Sb_{26.7}Te_{51.7}$	702	44	493	55	Q-A
21561-80	$Ag_{21.3}Sb_{26.3}Te_{52.4}$	702	44	493	55	Q-A
21561-81	$Ag_{20.9}Sb_{25.9}Te_{53.2}$	702	44	493	55	Q-A
21561-62	$Ag_{20}Sb_{25}Te_{55}$	693	40	500	42	Q-A
21561-59	$Ag_{1.01}Sb_{0.99}Se_2$	795[d]	46	590	48	FC-A
21561-3	$AgSbSe_2$	705	70	525	16	FC-A

(a) The elements were first heated at 500 to 600°C for several hours before heating to these temperatures.
(b) Quench-anneal.
(c) Furnace cool-anneal.
(d) Temperature increased to >950°C for several hours.

Properties. Approximate values of the Seebeck coefficient and resistivity (from hot-probe and four-probe measurements) of the zone levelled-zone refined $AgFeSe_2$ and $AgFeTe_2$ ingots are shown in Table 3. The erratic nature of the data is probably a result of the polyphase nature of the ingots.

TABLE 3. APPROXIMATE ELECTRICAL PROPERTIES[a] OF SOME TERNARIES

Ingot	Composition	Method[b] of Preparation	Approximate Seebeck Coefficient, μ V/°K	Approximate Resistivity, ohm-cm
21561-60	$AgFeTe_2$[c]	Q-A	-60 to -70	1.8 to 2.5×10^{-3}
21561-4	$AgFeTe_2$[c]	FC-A	-52 to -72	1.9 to 4.1×10^{-3}
21561-37	$AgFeTe_2$	ZL-R	-30 to -95	1.5 to 2.5×10^{-3}
21561-6	$AgFeSe_2$	FC-A	-8 to +80	3 to 8.5×10^{-3}
21561-49	$AgFeSe_2$	ZL-R	-60 to -85	1 to 2×10^{-3}
21561-3	$AgSbSe_2$[d]	FC-A	+50 to +500 (mostly +300 to +400)	4.4 to 4.7
21561-59	$Ag_{1.01}Sb_{0.99}Se_2$[d]	FC-A	+180 to +220	1.4 to 1.7×10^{-2}

(a) Thermoelectric hot-probe and four-probe data.
(b) FC-A: furnace cool-anneal; Q-A: quench-anneal; ZL-R: zone levelling - zone refining.
(c) Three phase.
(d) Single phase.

$AgSbTe_2$. During this period, study of the Ag-Sb-Te system was concerned with the effects of stoichiometry, degree of homogeneity, method of preparation, etc., on the thermoelectric properties. The studies conducted were concerned with (1) detailed metallographic examination, chemical and X-ray diffraction analysis, and measurement of electrical properties on selected specimens from the $AgSbTe_2$ ingot (No. 21561-16) prepared previously (First Quarterly Progress Report) by a combination of zone levelling and zone refining, and (2) the preparation and evaluation of specimens slightly off the 1:1:2 stoichiometry.

Homogeneity. Preliminary metallographic examination of polished sections removed at intervals along the zone levelled-zone refined ingot (No. 21561-16) had indicated that about 2 inches of the end first to crystallize was single phase, whereas the remainder of the ingot contained a minor second phase whose concentration increased progressively toward the tail of the ingot (end last to crystallize). However, more detailed metallographic examination (Figure 1) of material from near the head of the ingot (end first to freeze), etched in a 55 percent nitric acid solution for 30 seconds, revealed the presence of minute amounts of two minor phases. Total concentration of these minor phases was less than 1 percent (see Figures 1a, 1b, and 1c). (The black spots in the photographs are voids which were formed by chipping during polishing.)

X-ray examination of specimens removed at 0.7 (Specimen A) and 7.3 inches (Specimen B) from the end first to crystallize revealed that the major phase in both specimens was face-centered cubic with a lattice constant of 6.08 Å, the same as that reported in the literature for $AgSbTe_2$. However, the literature value probably may also have been obtained on samples containing minor phases. Specimen B contained a small amount of a second phase, but the pattern was too weak for the phase to be identified. The concentration of the minor phases observed optically in Specimen A was too low for detection by X-ray diffraction analysis.

The results of chemical analysis of specimens taken from the end first to freeze are shown in Table 4 (Samples 1, 4, and 6). Since the concentrations of the minor phases in this end of the ingot were very low, chemical analyses should give a good approximation to the composition of the major phase. It is seen that the silver concentration shows an increasing trend, whereas antimony and tellurium show a decreasing trend toward the end last to crystallize. Thus, some range of existence for the major phase is indicated. It may be noted that the stable composition is considerably different from stoichiometric $AgSbTe_2$. Although the composition of the major phase apparently changed along the ingot, the change in overall composition also coincides with a progressive increase in the concentrations of the minor phases. Samples 1, 4, and 6 contained minute amounts (~1 percent total) of two minor phases. Sample 8 (quenched) contained about 5 percent and Sample 9 about 10 to 20 percent of a minor phase.

Properties of Zone-Melted Ingot. Seebeck coefficient, resistivity, and Hall coefficient values were measured as functions of temperature from approximately 90 to 410°K on Samples 5', 7, 8, and 9. Sample 5' was removed between Samples 4 and 5 (Table 4) at 1.7 inches from the end first to freeze. The data are shown in Figures 2, 3, and 4. The resistivity and Hall coefficient varied monotonically with composition. The Seebeck coefficient was very insensitive to composition changes and/or the presence of small concentrations of minor phases, with the values for Samples 5', 7, and 8 differing by only a few percent at temperatures greater than approximately 200°K. (Sample 9,

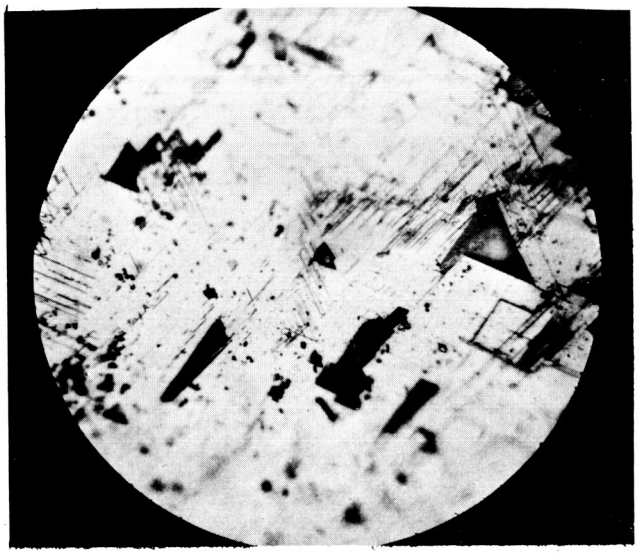

a. 0.5 Inch, Etched, ~0.3 Percent Minor Phase, 600X

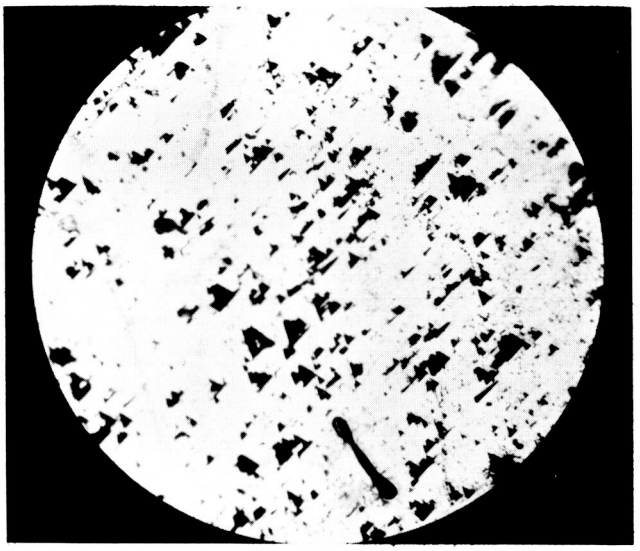

b. 0.5 Inch, Etched, ~0.3 Percent Minor Phase, 150X

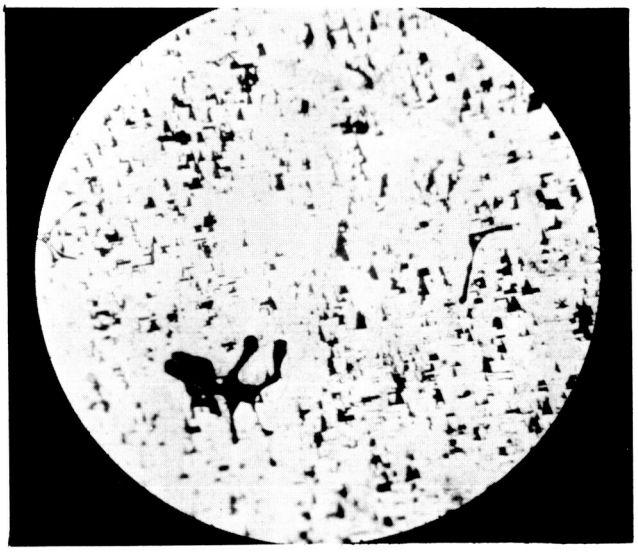

c. 2.1 Inches, Etched, ~1 Percent Minor Phase, 150X

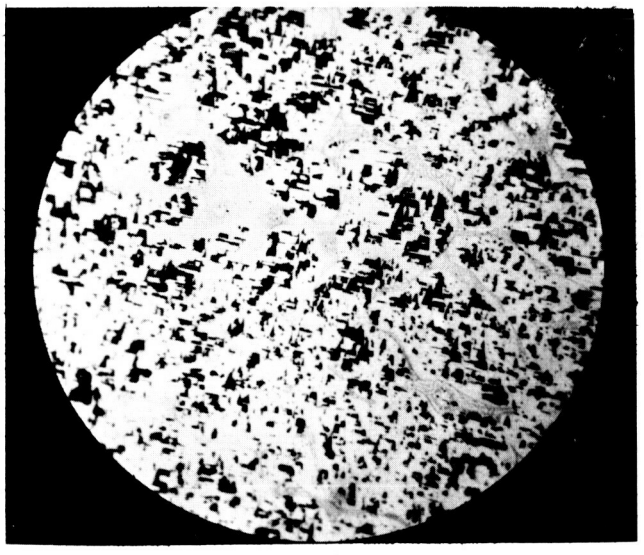

d. 4.0 Inches, ~3 Percent Minor Phase, 150X

FIGURE 1. METALLOGRAPHICALLY POLISHED SAMPLES OF ZONE LEVELLED-ZONE REFINED $AgSbTe_2$ [INGOT 21561-16 (a-f), DISTANCES ARE FROM END FIRST TO FREEZE] AND OF AIR QUENCHED-ANNEALED $AgSbTe_2$ [INGOT 21561-1, (g)]

Dark (black) areas are chips removed by lapping and polishing. One minor phase appears as needlelike inclusions in (a). The other minor phase is evident as gray stringers and spots in (d), (e), and (f), and appears as gray deposits along grain boundaries in (g).

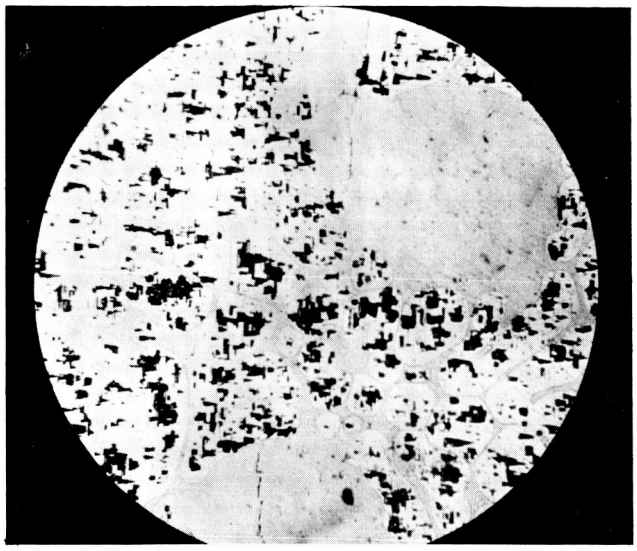

e. 5.9 Inches, ~10 Percent Second Phase, 150X

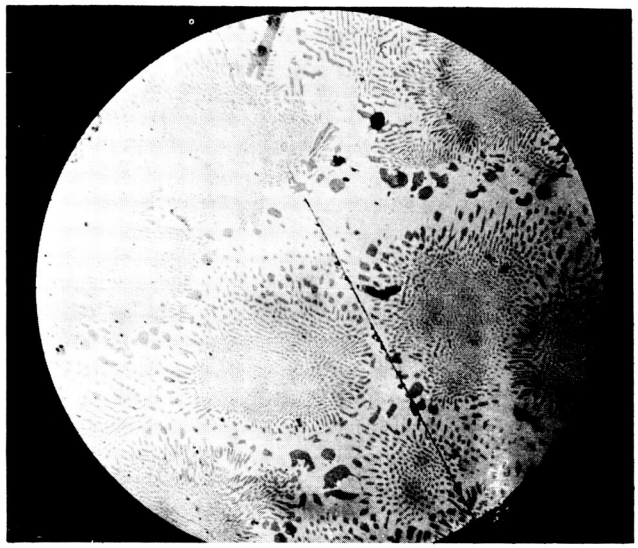

f. 5.9 Inches, ~25 Percent Second Phase, 150X

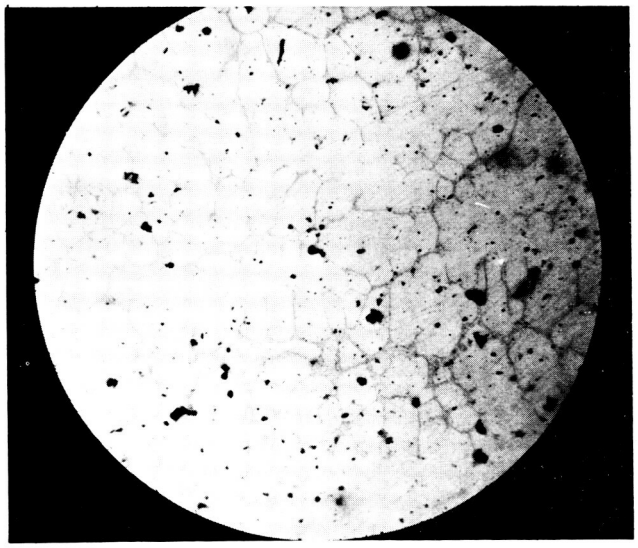

g. Quench-Anneal, ≈5 Percent Second Phase, 150X

FIGURE 1 (CONTINUED)

TABLE 4. COMPOSITION AND APPROXIMATE ELECTRICAL DATA

Sample	Ingot	Distance From End First to Freeze, D, inches	Composition, at. % Ag, x	Sb, y	Te, z	Composition Variables E[a]	A[b]
(1)	21561-16	0.3	20[d]	27.9[d]	52.1[d]	0.25	7.9
(2)	21561-16	0.5	--	--	--	0.5[e]	7.2[e]
(3)	21561-16	1.0	--	--	--	1.05[e]	5.7[e]
(4)	21561-16	1.1	21.3[d]	26.8[d]	51.9[d]	1.05	5.5
(5)	21561-16	2.0	--	--	--	0.5[e]	4.0[e]
(6)	21561-16	2.5	22.8[d]	26.3[d]	50.9[d]	0.05	3.5
(7)	21561-16	3.0	--	--	--	-0.4[e]	3.1[e]
(8)	21561-1	--	25	25	50	0	0
(9)	21561-16	>6	>25	<25	<50	--	--
(10)	21561-64	--	24	29	47	-8.5	5
(11)	21561-63	--	22	27	51	-0.5	5
(12)	21561-79	--	21.6	26.7	51.7	0.85	5
(13)	21561-80	--	21.3	26.3	52.4	2.3	5
(14)	21561-81	--	20.9	25.9	53.2	3.9	5
(15)	21561-62	--	20	25	55	7.5	5

(a) $E = z - \frac{x}{2} - \frac{3y}{2}$ = atomic percent of tellurium in excess of that in an alloy of Ag_2Te and Sb_2Te_3.

(b) A = y - x = atomic percent by which antimony exceeds silver in the alloy.
(c) All values positive.
(d) Obtained by chemical analysis.
(e) Extrapolated and interpolated values.
(f) Brown-colored second phase (metal rich).
(g) Gray-colored second phase (tellurium rich).

ON $Ag_xSb_yTe_z$ (WHERE x + y + z = 100) ALLOYS

Percent of Second Phase	Approximate Resistivity, ρ, ohm-cm	Approximate Seebeck Coefficient, S. $\mu V/°K$	S^2/ρ, watts/cm-deg^2	σ_o, ohm^{-1}-cm^{-1}
--	4.2×10^{-3}(e)	213(e)	10.5×10^{-6}(e)	370(e)
--	3.9×10^{-3}	215	11.9×10^{-6}	420
--	3.4×10^{-3}	220	14.2×10^{-6}	510
--	3.3×10^{-3}(e)	220(e)	14.4×10^{-6}(e)	520(e)
--	3.8×10^{-3}	225	13.3×10^{-6}	490
--	4.8×10^{-3}(e)	231(e)	11.2×10^{-6}(e)	410(e)
--	5.9×10^{-3}	235	9.4×10^{-6}	340
--	13×10^{-3}	250	4.8×10^{-6}	190
~80(f)	--	--	--	--
~30(f)	--	--	--	--
~1(g)	5.1×10^{-3}	135	3.7×10^{-6}	130
~4(g)	1.93×10^{-3}	82	3.4×10^{-6}	160
~10(g)	--	--	--	--
~20(g)	--	--	--	--

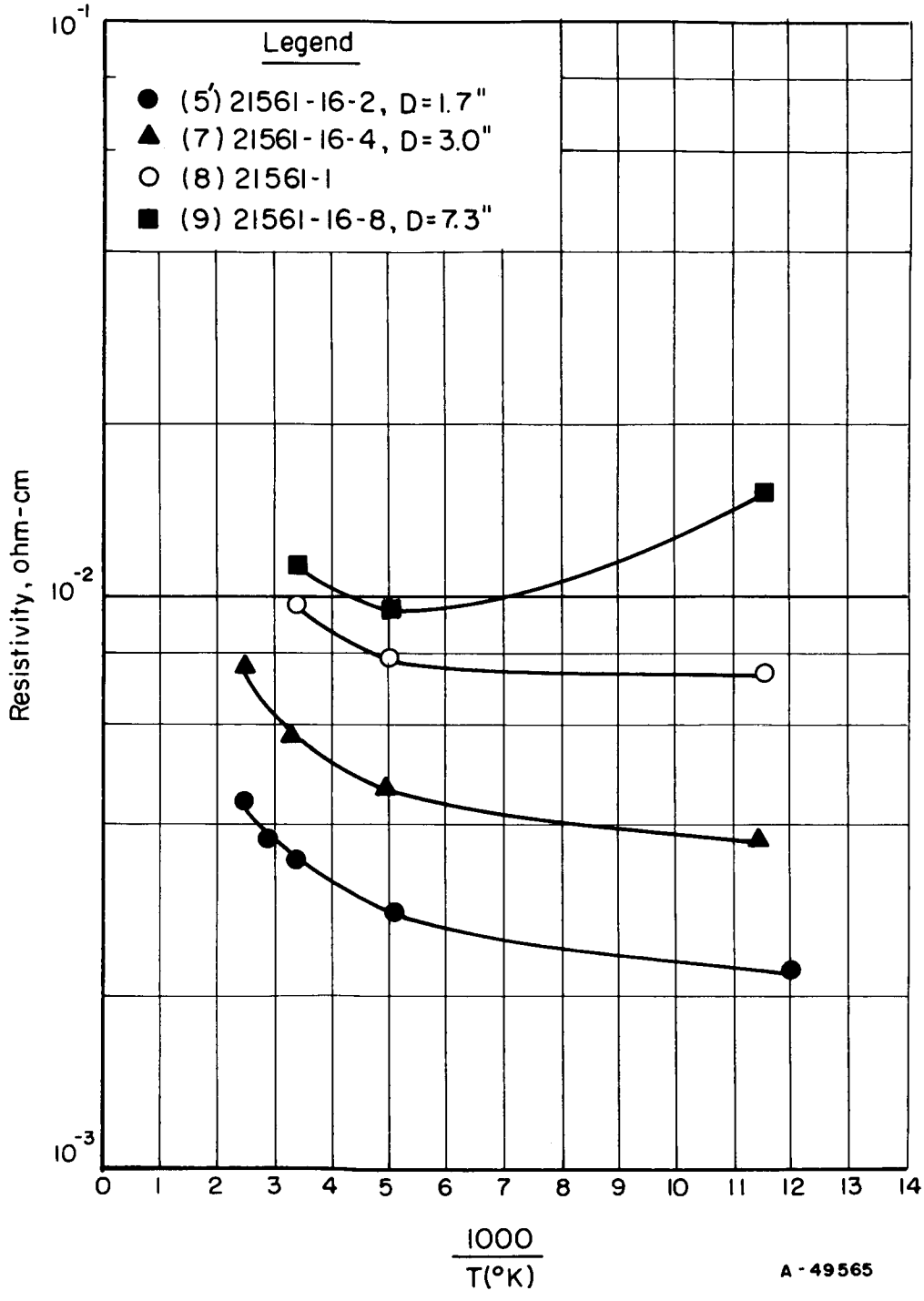

FIGURE 2. RESISTIVITY VERSUS RECIPROCAL TEMPERATURE FOR $Ag_xSb_yTe_z$ ALLOYS

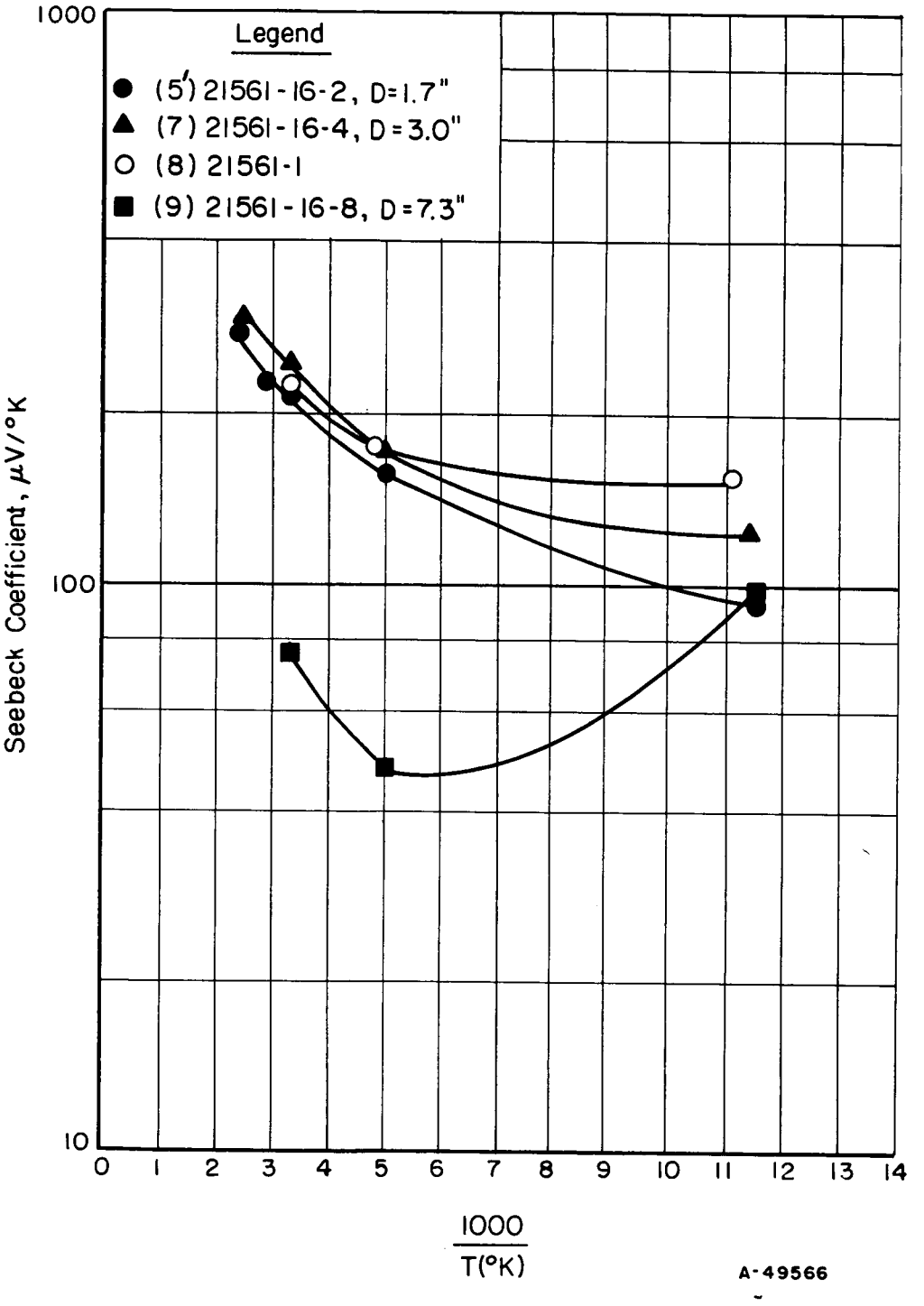

FIGURE 3. SEEBECK COEFFICIENT VERSUS RECIPROCAL TEMPERATURE FOR $Ag_xSb_yTe_z$ ALLOYS

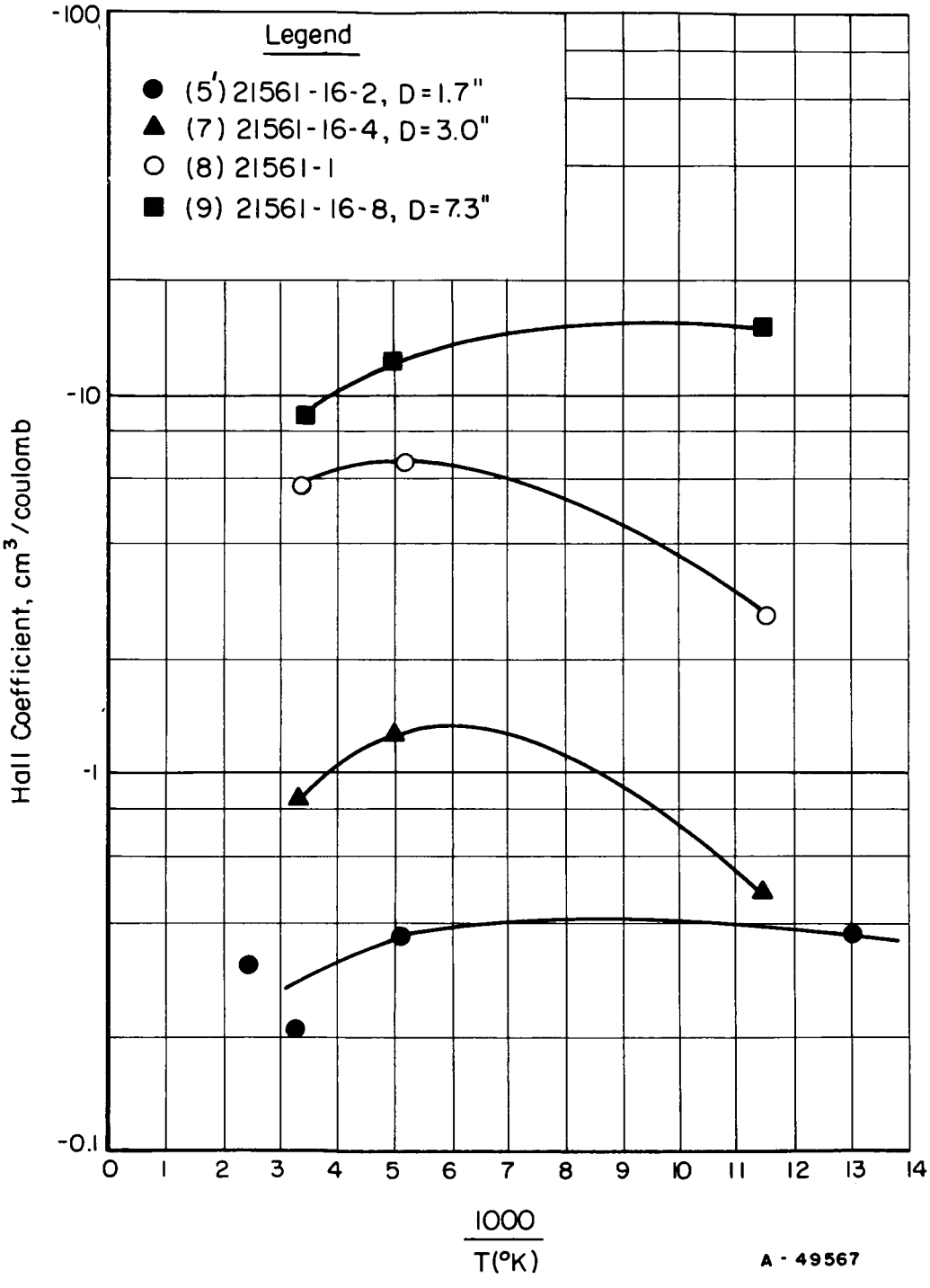

FIGURE 4. HALL COEFFICIENT AT 8000 GAUSS VERSUS RECIPROCAL TEMPERATURE FOR $Ag_xSb_yTe_z$ ALLOYS

which contained a large amount of a second phase, had a much lower Seebeck coefficient.) On the other hand, the resistivity varied by a factor of 3 from Sample 5' to Sample 8 and the Hall coefficient by a factor of 20. The reasons for these apparent inconsistencies are not yet known, but may be related to the presence of the minor phases.

Values of σ_o calculated* from the Seebeck coefficient and resistivity data are also shown in Table 4. Values of about 500 $ohm^{-1}-cm^{-1}$ were measured on specimens containing only traces of minor phase(s) (Samples 3, 4, and 5). Although it has been pointed out previously that thermoelectric-property measurements on such materials might be misleading, it is believed that the comparisons made and the trends noted here are valid even if absolute magnitudes of σ_o are in error.

The results for Ingots 21561-16 and 21561-1 indicate that considerable improvement in the thermoelectric properties of alloys in the Ag-Sb-Te system was attained by using the zone levelling-zone refining method of preparation rather than the quench-anneal method. Presumably, this improvement resulted from an increase in the homogeneity of the specimens. However, another variable which may also affect the electrical properties of these alloys is composition. Thus, a series of experiments designed primarily to determine the range of single-phase composition and the effect of composition on the thermoelectric properties of alloys in this system was conducted.

In the alloy system $Ag_xSb_yTe_z$, there are only two independent composition variables, since one of the variables can be expressed in terms of the other two. (For example, $z = 100 - x - y$ where x, y, and z are the atomic percentages of Ag, Sb, and Te, respectively.) Most previous researchers have chosen to consider this sytem as an alloy system of Ag_2Te and Sb_2Te_3. In this "pseudobinary system" there is only one independent variable, since an additional restraining equation can be written (for example, $z = x/2 - 3y/2 = 0$). It is convenient to consider as variables the percentage, A, by which the antimony concentration exceeds that of silver ($A = y - x$), and the atomic percentage, E, by which the tellurium concentration deviates from that in an alloy in the pseudobinary system ($E = z - x/2 - 3y/2$). These values for Ingot 21561-16 are given in Table 4. In general, higher values for either S^2/ρ or σ_o suggest better thermoelectric properties. For the zone levelled - zone refined ingot (No. 21561-16), it can be seen in Table 4 that S^2/ρ and σ_o have maxima at approximately the same composition at which E has a maximum. However, this does not necessarily indicate that the maximum in E is responsible for the maximum in S^2/ρ or σ_o since A is varying also and since the impurities may be concentrated at the end first to freeze. It would be desirable to know how S^2/ρ and σ_o vary as functions of E, with A and impurity concentrations remaining constant. Accordingly, six alloys (Samples 10 through 15 in Table 4) having A equal to 5** were prepared by the quench-anneal method as indicated in Table 3, and studies of metallographic and thermoelectric properties were made.

Metallographic examination revealed that all six alloys were polyphase. Sample 12 with E = +0.85 contained only a minor amount of a second phase (~1 percent). The other alloys contained from 4 to 80 percent of a second phase depending on the value of E. Because of the polyphase characteristic of these alloy specimens, no definite correlation could be made between composition and thermoelectric properties. However, it can be noted that the composition containing the lowest concentration of second phase is

*Assuming single carrier conduction and r = 0.

**The best thermoelectric properties were found previously in the vicinity of A equal to 5.

nearly identical with that (Sample 4) which gave best thermoelectric properties in the zone levelled-zone refined ingot. Also, it appears from these data that the stability region for essentially single-phase composition is very narrow. This is not in complete agreement with the data obtained on the ingot prepared by the zone levelling-zone refining method. Thus, additional work will be required to determine the reason for these differences and to establish a firm correlation between composition and thermoelectric properties.

Plans for this ternary system call for continued study of the effect of composition on the electrical properties of the Ag-Sb-Te alloys.

AgSbSe$_2$. Study of the effect of doping on the thermoelectric properties of AgSbSe$_2$ was started during this period. A single-phase ingot with a nominal composition of $Ag_{1.01}Sb_{0.99}Se_2$ (No. 21561-59) was prepared by the furnace cool-anneal method under the conditions shown in Table 2. Preparative conditions for this ingot differ somewhat from those for the undoped ingot of AgSbSe$_2$ (Ingot No. 21561-3, First Quarterly Progress Report) in that the doped ingot was reacted and annealed at higher temperatures. Although the Seebeck coefficient of the doped ingot was lower than that of the undoped one, the resistivity was decreased by several orders of magnitude by doping, with a resultant increase in S^2/ρ at 300°K from 6.7×10^{-8} to 2.6×10^{-6} μV^2/ohm-cm°C and a corresponding increase in σ_o from 8 ohm^{-1}-cm^{-1} for the undoped specimen to 90 ohm^{-1}-cm^{-1} for the doped specimen. Although the σ_o value for the doped material is still very low, the improvement effected by doping suggests that the compound merits further study. Specimens prepared thus far have been polycrystalline; grain-boundary effects may have affected the properties.

Plans for this ternary call for further doping studies and attempts to improve crystallinity.

Bismuth-Antimony Alloys. Study of the $Bi_{86}Sb_{14}$ alloy for thermoelectric applications at low temperatures was continued. Emphasis was placed on (1) preparing both n-type (undoped and tellurium doped) and p-type (tin doped) alloys, (2) measuring Seebeck-coefficient and resistivity values on single-crystal specimens as functions of temperature and (3) studying the homogeneity of the alloys.

The alloys containing approximately 14 atomic percent antimony were chosen for initial study because it has been reported that this composition has about the maximum energy gap (0.024 ev) in the Bi-Sb alloy system.[4] All other variables being equal, the alloy with the largest band gap would have the highest figure of merit, since the contribution of ambipolar diffusion to the thermal conductivity as well as the partial cancellation of the Seebeck coefficient by minority carriers would be minimized.

Preparation. The alloy ingots listed in Table 5 were prepared during this study. These were prepared by zone levelling at a crystallization rate of 3.2 cm per hour, using rf induction heating and coupling directly to the melt. A carbon-coated quartz boat of semicircular cross section was used as the melt container. (The coating reduced stray nucleation at the melt-container interface.)

The preparation procedure was as outlined in the First Quarterly Progress Report. Polycrystalline ingots were prepared for zone levelling by the specially developed

decanting technique to eliminate oxides from the surface of the ingots. In the preparation of the doped ingots, the dopant was added to the bismuth and antimony prior to casting of the polycrystalline ingots.

TABLE 5. COMPOSITION OF BISMUTH-ANTIMONY ALLOYS

Ingot	Nominal Composition, atomic percent			
	Bi	Sb	Te	Sn
21590-1	86	14	--	--
-5	82.8	13.8	--	3.4
-18	84.2	14.0	1.8	--
-27	84.1	14.0	--	1.9
-31	84.9	14.2	0.9	--
-45	85.5	14.3	0.2	--
-47	85.5	14.2	--	0.2

Each ingot, weighing approximately 375 g and measuring about 2.2 cm by 25 cm, was given 12-30 zone-levelling passes.

Whenever possible, seeding was used to control the orientation of the principal cleavage plane (plane perpendicular to the c-axis). This was necessary in order to obtain specimens with the desired dimensions (16-20 mm by 4-5 mm by 2-4 mm) for evaluation. If the orientation was not controlled, the cleavage plane was generally oriented at 45° to 60° with respect to the longitudinal axis of the ingot and tilted with respect to the vertical axis. Examples of three ingots of doped and undoped $Bi_{86}Sb_{14}$ alloy are shown in Figure 5. In Figure 5a, the cleavage plane, controlled by seeding, was oriented vertically and perpendicular to the longitudinal axis (growth axis) of the ingot. In the other ingots, the cleavage planes were as shown in the photographs.

Electrical Measurements. In earlier work on determining the electrical properties of an n-type, undoped $Bi_{85.4}Sb_{14.6}$ alloy specimen (Specimen 21590-1), it was observed that the values measured before and after Z-meter measurements did not agree. Those obtained prior to Z-meter measurements were in good agreement with the Z-meter values at 300 and 80°K. However, those obtained after Z-meter measurements were made differed from initial properties (Figure 6, Curves 1 and 2), especially at low temperatures. Since this specimen had been contacted three times, the results suggested that the sample had been inadvertently doped or otherwise altered in the contacting process.

Another specimen (No. 21590-1B) was removed from the same ingot, and Seebeck coefficient and resistivity values were measured as functions of temperature. Electrical contact was made to the specimen with In-Bi solder applied ultrasonically, as had been

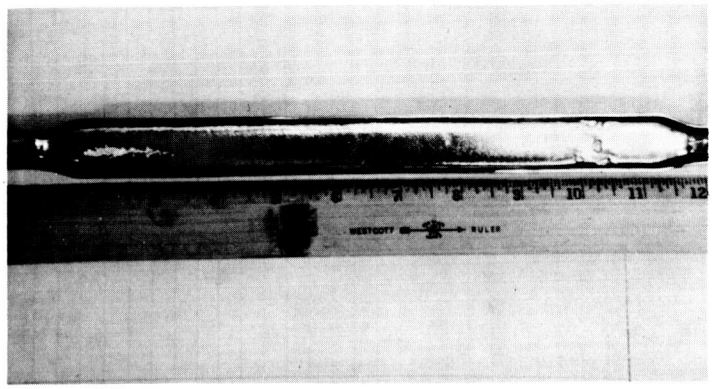

a. N-Type (Undoped)

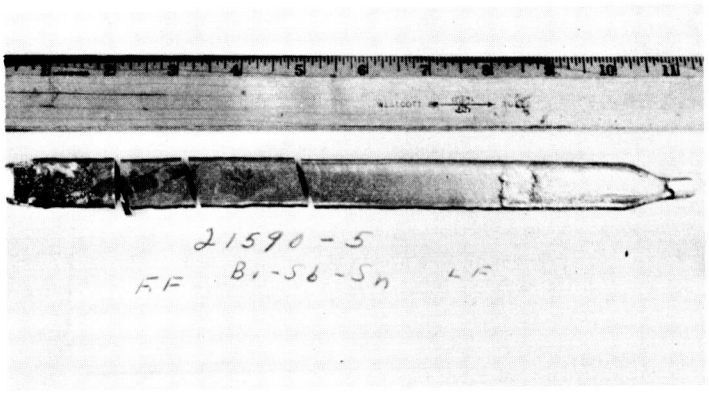

b. P-Type (Sn Doped)

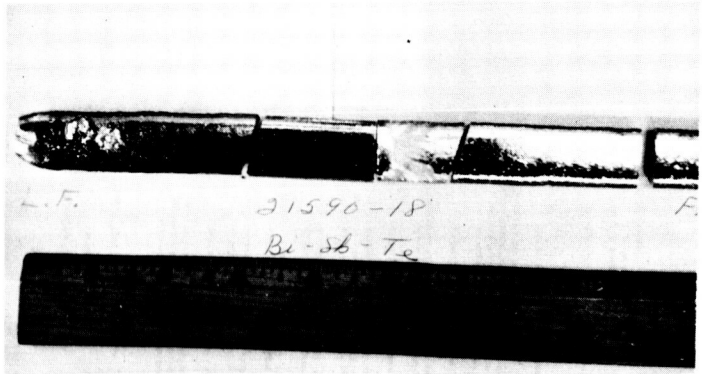

c. N-Type (Te Doped)

FIGURE 5. Bi-Sb ALLOY INGOTS

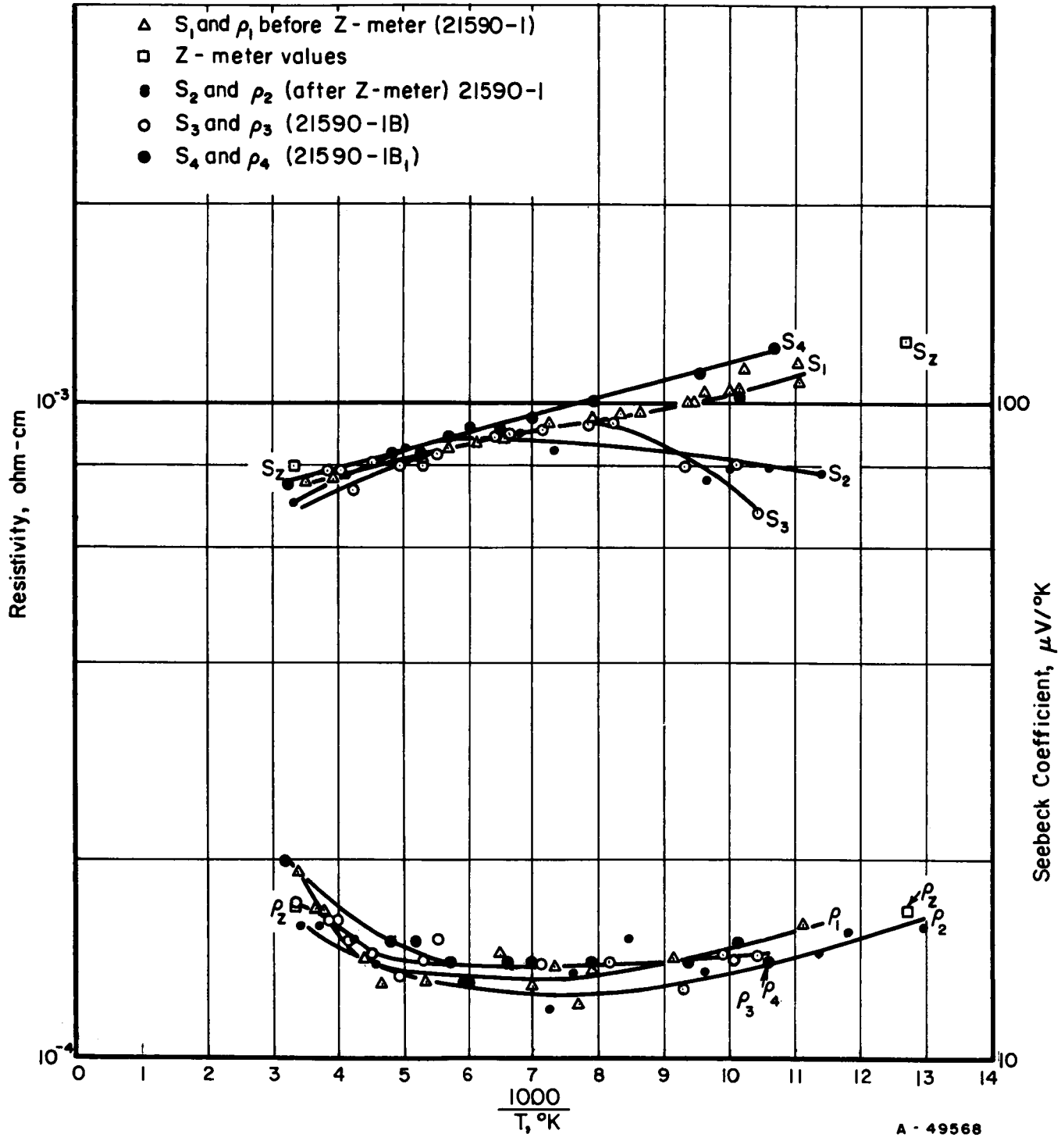

FIGURE 6. SEEBECK COEFFICIENT AND RESISTIVITY VERSUS RECIPROCAL TEMPERATURE FOR (N-TYPE, UNDOPED) $Bi_{85.4}Sb_{14.6}$ ALLOY

done with the other specimen prior to making Z-meter measurements. As seen in Figure 6, Curve 3, the Seebeck coefficient values above 125°K agreed with those obtained on the previous specimen before Z-meter measurements were made. However, below 125°K the Seebeck coefficient of the latter specimen decreased, rather than increasing as expected. A similar behavior, to a lesser degree, was observed in the resistivity.

Sample 21590-1B was recontacted and remeasured. The old end contacts were removed by cleaving off any damaged or contaminated area, and new contacts were applied. The new contacts (In-Bi eutectic solder) were applied using only a soldering pencil and as low a temperature as possible. It was noted that the Seebeck coefficient values (Curve 4) for the recontacted specimen (No. $21590\text{-}1B_1$) were the same, within experimental error, as those of Specimen 21590-1 before Z-measurements over the entire temperature range, and they also agreed with the Z-meter values at 300 and 80°K. Apparently, applying the In-Bi eutectic solder at high temperatures affected the electrical properties of the Bi-Sb specimens, possibly by alloying the solder with the specimens.

Seebeck coefficient and resistivity values were measured as functions of temperature on several doped (p- and n-type) and undoped (n-type) single-crystal (Figure 6) $Bi_{86}Sb_{14}$ alloy specimens. The values were measured along the trigonal axis, the direction of maximum figure of merit. Electrical contact was made to the specimens with In-Bi solder, using a soldering pencil and as low a temperature as possible to prevent attack of the specimens by the solder. The data obtained on the doped ingots are shown in Figures 7 and 8. The Seebeck coefficient values were low for all three specimens, indicating that they were overdoped. The values for Specimen 21590-27 (1.9 percent tin) exhibited a crossover at about 300°K, whereas the Seebeck coefficient for the other tin-doped specimen (No. 21540-5B) showed indications of a crossover at a higher temperature. Reducing the amount of tin from 3.4 atomic to 1.9 atomic percent increased the Seebeck coefficient and the value of S^2/ρ slightly.

Evaluation of ingots containing smaller concentrations of dopants is in progress.

Homogeneity. A high degree of inhomogeneity in a material generally leads to a lower figure of merit than if the material is homogeneous. The lower figure of merit for an inhomogeneous material results from an increase in the thermal conductivity and a decrease in the Seebeck coefficient by the circulating-current effect, as discussed in the First Quarterly Progress Report. Thus, it is expected that the figure of merit of a material can be improved by improving the homogeneity.

In several alloy systems – including the Bi-Sb alloy system – it has been observed that single crystals exhibit a cellular-like structure. In a series of decanting and etching studies along with electron-microprobe analyses conducted on the $Bi_{95}Sb_5$ alloy at Battelle, it was determined that this cellular-like structure represented a high degree of inhomogeneity. The center of the cells, triangular pyramids extending from the crystallizing interface into the melt, was richer in antimony than the cell walls.

During this report period, preliminary metallographic examinations were made of several $Bi_{86}Sb_{14}$ alloy specimens, doped and undoped, to determine the degree of inhomogeneity present.[5]* Examinations were conducted on the cleavage plane (plane perpendicular to the trigonal axis).

*The alloy specimens were examined by an electrolytic etching technique.[4,5] Single-crystal cleaved specimens were mounted in Kold-Weld potting compound and mechanically polished. The polished specimens were then electrolytically etched using a mixture of 20 parts methyl alcohol, 5 parts H_2SO_4, 5 parts HCl, and 2 parts ethylene glycol as the electrolyte. The etched surface was then electrolytically stained using a 5 percent aqueous chromic acid solution as the electrolyte. Platinum was used as the electrodes. Contact was made to the specimens using the platinum anode.

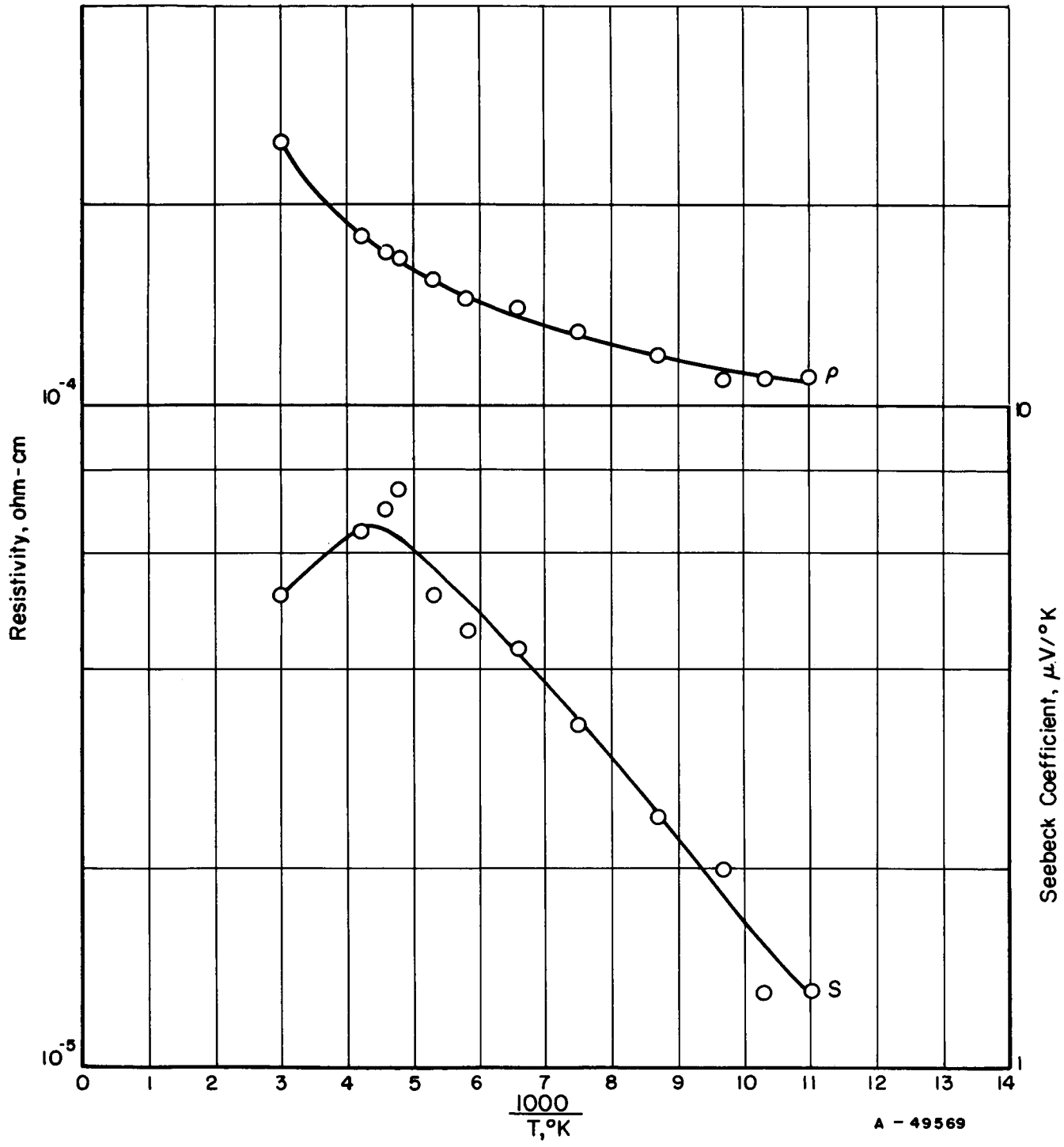

FIGURE 7. SEEBECK COEFFICIENT AND RESISTIVITY VERSUS TEMPERATURE FOR N-TYPE, Te-DOPED $Bi_{86}Sb_{14}$ ALLOY (21590-78)

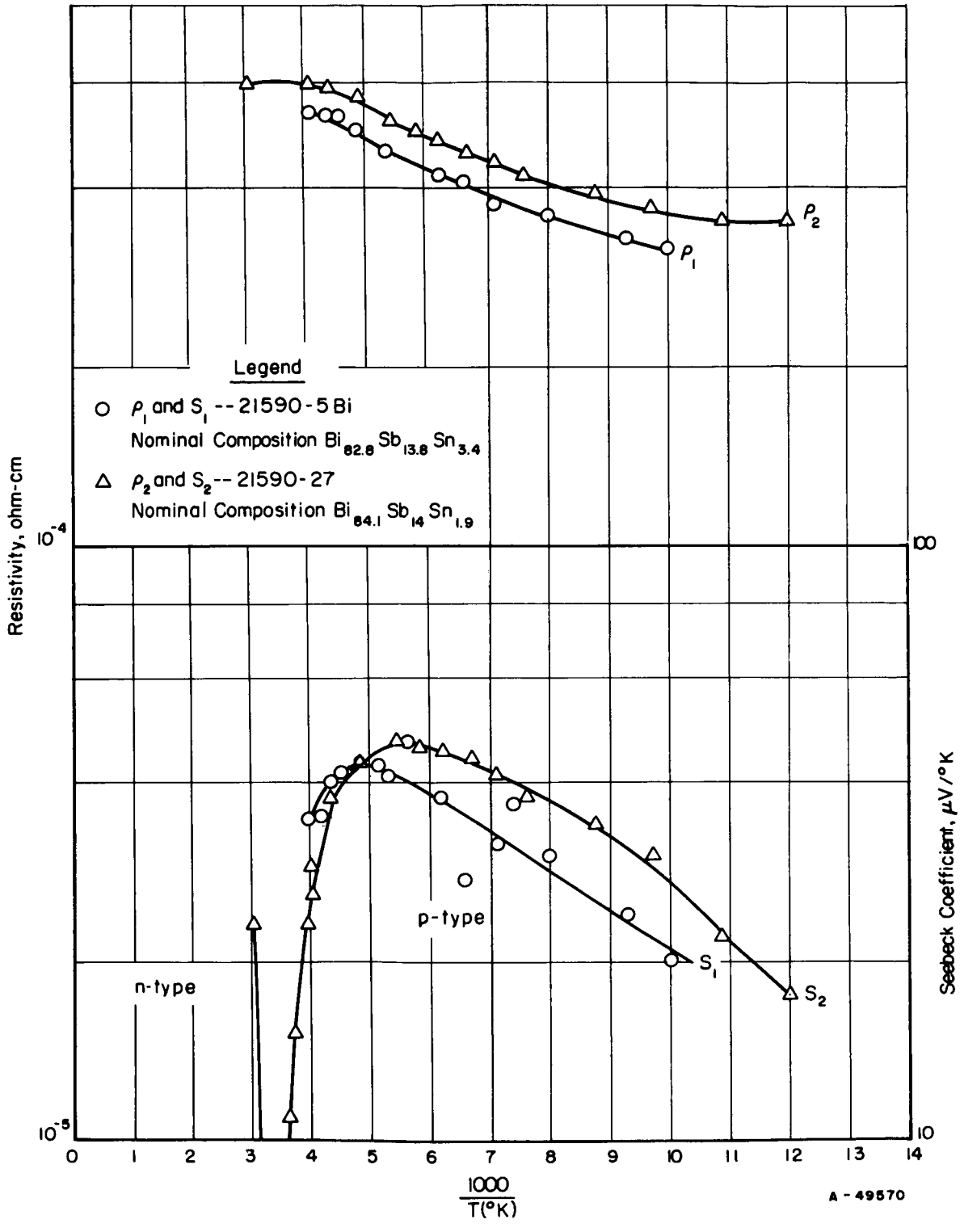

FIGURE 8. SEEBECK COEFFICIENT AND RESISTIVITY VERSUS RECIPROCAL TEMPERATURE FOR P-TYPE (Sn DOPED) $Bi_{86}Sb_{14}$ ALLOYS

Each of the Bi-Sb alloy specimens prepared to date under this contract was found to contain randomly oriented cells. From the structures on the etched surfaces as seen in Figure 9, some of the cells appeared to be oriented perpendicular to the cleavage plane (two triangular structures in lower half of Figure 9a), whereas other cells within the same specimen appeared to be oriented at some angle other than perpendicular to the cleavage plane (cross hatch in Figure 9b). It is expected that this cellular-like structure represents a degree of inhomogeneity which may have a detrimental effect on the electrical properties of the alloys.

Theoretical Investigations

Introduction

In order to further the primary objective of the theoretical investigations phase of this research program, the establishment of useful criteria for the selection and development of improved thermoelectric materials, it is desired to determine the magnitude of the maximum figure of merit that can be obtained with a given material with respect to variations in alloy composition, impurity doping, and temperature. This maximum figure of merit is the significant quantity to consider in attempting to establish possible criteria for preselecting potentially superior thermoelectric materials. This report will be concerned primarily with optimizing the figure of merit with respect to impurity doping and temperature, but with some preliminary considerations also introduced with regard to alloying.

The term "figure of merit", wherever used in the theoretical investigations section of this report, is taken to mean the dimensionless thermoelectric figure of merit, ZT, where $Z \equiv S^2\sigma/K$ is the figure of merit as ordinarily defined, T is the absolute temperature, S is the Seebeck coefficient, σ is the electrical conductivity and K is the thermal conductivity. The various performance measures of thermoelectric devices are usually functions of ZT rather than of Z alone. The value of ZT when optimized with respect to impurity doping at a given temperature will be designated as Z(max)T, in agreement with previously established notation. When optimized with respect to both impurity doping and temperature, the notation $(ZT)_{max}$ will be employed.

According to the parabolic, single-energy-band model discussed in the First Quarterly Progress Report, Z(max)T is a function only of the material parameter β and the scattering parameter r, approximately in the combination β exp r. The designation "single energy band" includes the case of a multiplicity of equivalent energy extrema located at crystal symmetry points in the Brillouin zone. Since Z(max)T increases monotonically with β, and if the latter is an increasing function of temperature, as is ordinarily the case, the single-band model would predict that $(ZT)_{max} = \infty$. Thus, the single-energy band model is inadequate for obtaining the value of $(ZT)_{max}$. As the temperature is increased, the thermally activated minority carriers begin to limit the value of Z(max)T because of their adverse effects on the Seebeck coefficient and on the thermal conductivity. The density of minority carriers can always be suppressed, of course, by increasing the impurity doping within the limits of solubility of impurities in the crystal lattice. However, too high a concentration of majority carriers would also affect ZT adversely. Consequently, when the temperature is increased beyond a certain point, the value of ZT will begin to decrease with increasing temperatures despite the continued increase in β with temperature and despite the best compromise that can be made in the

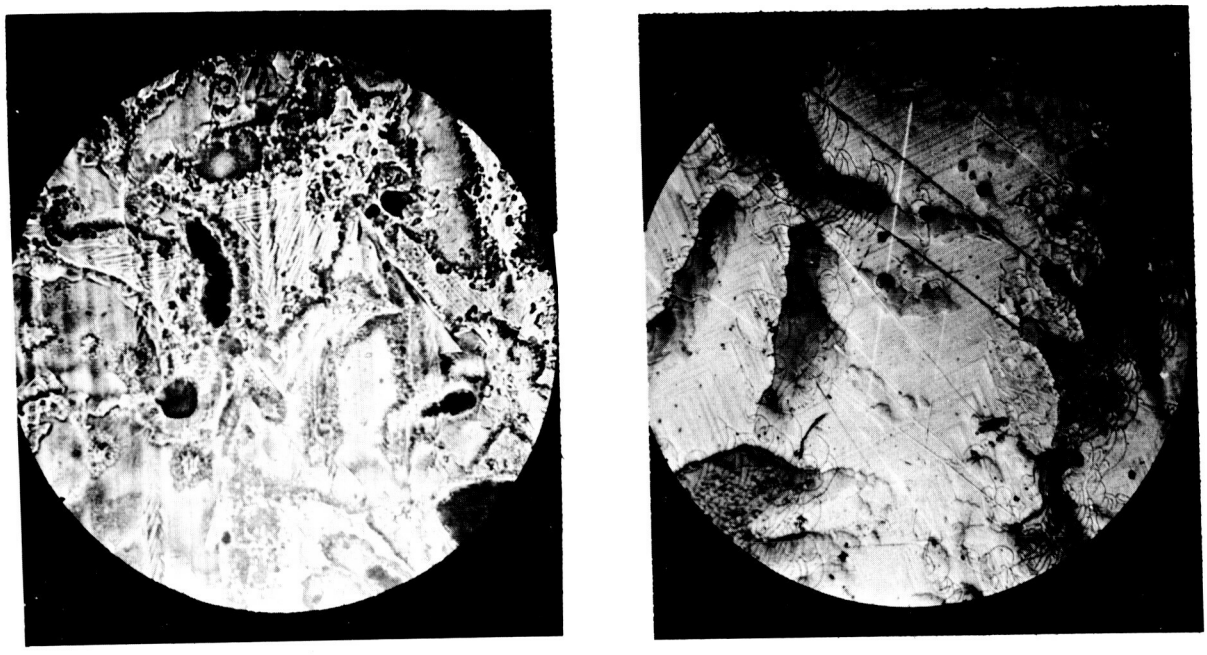

a. Cells Perpendicular to Cleavage Plane, 150X

b. Cells Not Perpendicular to Cleavage Plane

FIGURE 9. CELLULAR GROWTH IN Bi_{86} Sb_{14} ALLOYS

level of impurity doping to suppress minority carrier effects and simultaneously avoid the deleterious effects of too high a majority carrier concentration. The value of Z(max)T at this point in temperature is $(ZT)_{max}$.

The determination of the value of $(ZT)_{max}$ requires the use of at least a two-band (conduction band plus valence band) model of thermoelectric materials. The pertinent features of the theory and results of previous considerations of the two-band model will be reviewed briefly in this report. The results of new calculations of the values of Z(max)T that cover much wider ranges of values of the several pertinent parameters of the two-band model than have been covered heretofore are presented and discussed in this report. The method for obtaining the value of $(ZT)_{max}$ for a given material from the known temperature variations of the various parameters of the two-band model is also treated.

The values of the two-band model parameters are computed and tabulated for the common elemental and binary compound semiconductors for which the necessary data were found in the literature. Although most of these materials have a more complex energy-band structure, characterized by a multiplicity of either or both conduction and valence bands, and often with strongly nonparabolic relationships between energy and wave number vector, it is possible to formulate approximately equivalent two-band models that are useful for the $(ZT)_{max}$ considerations. Some preliminary observations are made on the results of these computations.

The Two-Band Model

Résumé of Theory. The two-band model consists of a single conduction band plus a single valence band separated by an energy gap, E_G. The position of the Fermi energy level is adjusted by impurity doping to the value E_F, as measured positively upward from the conduction band minimum. The Fermi energy, as measured positively downward from the valence band maximum, is then given by $-E_F - E_G$.

The thermoelectric figure of merit for the two-band model material, doped to obtain a negative Seebeck coefficient as used for the n-type leg of a thermocouple, is given by

$$ZT = (\gamma A_e B_e + \gamma^{-1} A_h B_h)^2 / [(\gamma \beta_e^{-1} + \gamma L_e B_e + \gamma^{-1} L_h B_h) \cdot (\gamma B_e + \gamma^{-1} B_h) + (A_e - A_h)^2 B_e B_h] \quad . \tag{1}$$

Equation (1) is obtained by combining Equations (19) and (20) of Reference (2), in which the theory of the thermoelectric figure of merit of two-band semiconductors is developed. In Equation (1),

$$A_e = - \left[\frac{r+2}{r+1} \frac{F_{r+1}(\eta_e)}{F_r(\eta_e)} - \eta_e \right] \quad , \tag{2}$$

$$B_e = F_r(\eta_e)/r! \quad , \tag{3}$$

and $$L_e = \frac{r+3}{r+1}\,\frac{F_{r+2}(\eta_e)}{F_r(\eta_e)} - \left[\frac{r+2}{r+1}\,\frac{F_{r+1}(\eta_e)}{F_r(\eta_e)}\right]^2 \quad . \tag{4}$$

A_h, B_h, and C_h are defined similarly, with η_h substituted for η_e and the sign of A_h positive instead of negative. B_h and L_h do not change sign. $\eta_e = E_F/kT$ is the reduced (dimensionless) Fermi energy for electrons and $\eta_h = -\eta_e - \eta_G$ is the reduced Fermi energy for holes, where $\eta_G = E_G/kT$ is the reduced band gap. $F_r(\eta)$ is the standard Fermi integral and r is the scattering parameter, the exponent in the assumed power law relationship between the mean free path and the energy of the charge carrier. The quantity β_e is the dimensionless material parameter pertinent to the conduction band, namely

$$\beta_e = (k/e)^2\,\sigma_{oe}T/K_L \quad , \tag{5}$$

where $k/e = 86.2 \times 10^{-6}$ V/°C is the ratio of Boltzmann's constant to the magnitude of the electronic charge, K_L is the lattice contribution to the thermal conductivity and σ_{oe} is given by

$$\sigma_{oe} = 2N_e(2\pi m_d\, kT/h^2)^{3/2}\, e\mu_{ce} \quad . \tag{6}$$

In Equation (6), N_e is the number of equivalent valleys in the conduction band, $m_d = (m_1 m_2 m_3)^{1/3}$ is the density-of-states mass per valley, where m_1, m_2, and m_3 are the three principal electron effective masses, h is Planck's constant, and μ_{ce} is the low-carrier-concentration (classical statistics) value of the electron mobility. μ_{ce} is isotropic for crystals of cubic symmetry and is given by $(1/3)(\mu_1 + \mu_2 + \mu_3)$, where μ_1, μ_2, and μ_3 are the partial mobilities[6] associated with the three principal directions of each energy ellipsoid. For crystals of lower symmetry than cubic, the quantity $N_e\mu_{ce}$ is obtained by summing up the expressions $(\lambda_{1x}^2\,\mu_1 + \lambda_{2x}^2\,\mu_2 + \lambda_{3x}^2\,\mu_3)$ over all energy ellipsoids, where λ_{1x} is the direction cosine between the principal axes (1) and the current direction (x), etc. Finally, the quantity γ in Equation (1) is defined by

$$\gamma \equiv (\beta_e/\beta_h)^{1/2} = (\sigma_{oe}/\sigma_{oh})^{1/2} \quad . \tag{7}$$

The quantity ZT as given by Equation (1) exhibits, in general, two maxima as a function of η_e, one corresponding to optimum doping for the n-type material and the other to optimum doping for the p-type material. ZT approaches zero for either high positive or high negative values of η_e (corresponding to high negative or high positive values of η_h, respectively) and also vanishes at the point between the two maxima where the Seebeck coefficient changes sign, i.e., when $\gamma A_e B_e + \gamma^{-1} A_h B_h = 0$. We will designate by Z(max)T only the first one of these maxima, the one for n-type material. No generality is lost in so doing, since the value of the p-type maximum could also be found by considering only the first maximum by replacing β_e by β_h and γ by its reciprocal in Equation (1). This formalism avoids the inconvenience of having to represent Z(max)T as a double-valued rather than as a single-valued function of the two-band parameters, β, γ, η_G, and r. The same value of r is assumed here to apply to both electrons and holes.

The analytical procedure used for determining the value of Z(max)T for a given set of values of β, γ, η_G, and r is to compute ZT for a series of three equally spaced values of η_e about its optimum value, such as $\eta_e = +1$, 0, and -1. Over most of the ranges of values of the above parameters of interest, the optimum Fermi level lies within ±1 kT from the band edge. However, computations of ZT for values of $\eta_e > +1$ are needed for

small β's or for small or negative (semimetallic conduction) values of η_G and values of $\eta_e < -1$ are needed for large values of β and η_G. The ZT maxima are usually broad enough so that the value of Z(max)T can be determined to a sufficient degree of accuracy (two significant figures) from the three consecutive ZT values corresponding to unit changes in η_e by parabolic interpolation. It is readily shown that if $(ZT)_2$ is the largest one of the set of three consecutive values $(ZT)_1$, $(ZT)_2$, and $(ZT)_3$, then if the portion of the ZT versus η_e curve in this neighborhood is approximated by a parabola passing through these three points, we have

$$Z(\max)T = (ZT)_2 + \frac{[(ZT)_1 - (ZT)_3]^2/16}{(ZT)_2 - (1/2)[(ZT)_1 + (ZT)_2]} \quad . \tag{8}$$

The results of computations of Z(max)T are given in Reference (1) for a few combinations of values of β, γ, η_G, and r that lead to Z(max)T values in the range 1 to 2. The best thermoelectric materials available today at any temperature have ZT values in the neighborhood of unity or somewhat above. It was of interest in Reference (2) to ascertain what would be required in the way of values of these parameters to obtain ZT values ranging up to 2. For the purpose of the $(ZT)_{max}$ considerations to be presented in this report, it was desired to obtain Z(max)T as a function of these parameters over a much wider range of Z(max)T values. Consequently, computations were made of Z(max)T, using Equations (1) and (8), for values of β_e ranging from 1/32 to ∞, of γ^2 ranging from 1/2 to 4, of η_G ranging from -4 to +8 and for r = 0 (acoustical-mode lattice vibration scattering of the charge carriers) and for r = 1 (optical-mode lattice vibration scattering)*.

Z(max)T Relationships. Figure 10 shows the results of the above calculations for the case of r = 0, in the form of a series of curves of Z(max)T as a function of β for various values of η_G and γ. Figure 11 shows the analogous results for the case of r = 1 but with 2.718 β (= β exp r for r = 1) plotted along the abscissa. The upper limiting curves of Figures 10 and 11 correspond to the single-band case, for which Z(max)T is approximately a function of the combination β exp r. These upper limiting curves are the same as shown in Figure 8 of the First Quarterly Progress Report. The single-band case is obtainable from Equation (1) if either η_G or γ is set equal to infinity. It is evident from Figures 10 and 11 that the greater the value of the material parameter β, the greater must be the actual magnitude of either η_G or γ for either of them to be effectively infinite; that is, for the single-band Z(max)T value to be approximated. This is one of the reasons why it is increasingly difficult to find thermoelectric materials with higher Z(max)T values; they must have higher values of both β and η_G or γ.

With the aid of Figures 10 and 11 it is possible to assess more expeditiously the effectiveness of various measures taken to attempt to improve the ZT value of a given material. For example, alloying with an increasing percentage of a miscible compound may serve to increase β but to decrease η_G and γ. Use of the curves in these figures would then indicate if there would be any net gain or loss in the value of Z(max)T with increasing alloy composition. If there is an initial net gain, it could be determined what alloy composition, if any, would be optimum. Determination of the feasibility of obtaining optimum doping could then be made with the optimum alloy composition, assuming that the predicted Z(max)T value is high enough to justify the further experimentation.

Comparison of Figures 10 and 11 seems to indicate a distinct advantage of r = 1 over r = 0, not only because Z(max)T depends approximately on the combination β exp r

*These computations were made at no cost to the project with the aid of the Battelle digital computer facilities as a practice problem in connection with an instruction course in FORTRAN attended by one of the project personnel.

but also because the low values of η_G have much less of a deleterious effect on Z(max)T for r = 1 than for r = 0. Optical-mode lattice scattering may thus be advantageous for materials with small band gaps or band overlaps despite the accompanying decrease in β for this scattering mode; this is particularly so in the region where Z(max)T is insensitive to the value of β. The relationship between Z(max)T and β, γ, and η_G becomes insensitive to the value of r, however, in the upper right-hand region of these curves of Figures 10 and 11, corresponding to as-yet-unobtained larger values of Z(max)T.

It is to be noted that the various curves of Figures 10 and 11 for finite values of η_G and γ^2 approach constant values of Z(max)T as β increases indefinitely, indicating that Z(max)T becomes insensitive to further increase in the value of the material parameter beyond a certain point, unless, as previously noted, η_G or γ^2 are also increased. Setting $\beta = \infty$ in Equation (1) results in the variation of ZT with η_e for a hypothetical material with an essentially zero lattice component of thermal conductivity. The wide ranges of conditions under which the curves of Figures 10 and 11 are almost horizontal indicate that K_L would be much less than $K_{e\ell}$ at optimum doping under many circumstances (where $K_{e\ell}$ is the electronic component of the thermal conductivity).

Setting $\beta_e = \infty$ in Equation (1) and solving for Z(max)T as a function of η_G, γ, and r results in the family of curves of Figure 12. If the minority carrier were not activated, ZT would increase indefinitely with decrease in η_e for $K_L = 0$, since the Seebeck coefficient increases with decrease in η_e but the ratio of σ to $K_{e\ell}$ approaches a constant. However, the increase in concentration of the minority carriers (holes) with decrease in η_e begins to limit the further increase in the Seebeck coefficient and also decreases the ratio of σ to $K_{e\ell}$ through the increase in heat transport by ambipolar diffusion, represented by the last term in the denominator of Equation (1). In ambipolar diffusion, the excess of electron-hole pairs that are thermally activated at the hotter end of the semiconductor specimen over those thermally activated at the colder end drift down the temperature gradient and recombine toward the colder end, thus providing an additional heat-transport mechanism with accompanying zero net charge transport. It is to be noted that the curves of Figure 12 are plotted in the form of Z(max)T as a function of $\eta_G + 2r$. This results in approximate superposition of the curves for r = 0 and r = 1, corresponding to the same values of γ in the region of about $1 \leq Z(max)T \leq 2$. Although in this region Z(max)T is approximately a function of the combination of $\eta_G + 2r$, as noted in Reference (2), this is a poor approximation elsewhere. Z(max)T is less sensitive to r near the upper end of the curves and is much more sensitive to r at the lower end.

It is seen on Figure 12 that the four curves for r = 0 are almost parallel to one another and, except in the region of $\eta_G = -4$, are separated from each other horizontally by a value of $\Delta\eta_G$ ranging from about 0.8 to 1.2. Little error is made as far as the value of Z(max)T is concerned by assuming that doubling γ^2 is equivalent to increasing the reduced energy gap by one unit. Figure 10 shows that the same conclusion applies to finite values of β as well as to $\beta = \infty$. The curves for r = 1 are also almost parallel but with a somewhat closer average horizontal spacing of about $\Delta\eta_G = 0.8$. Hence, over a wide range of values of γ and η_G, Z(max)T is to a good approximation a function of $\eta_G + 2.89 \ln\gamma$ for r = 0 and of $\eta_G + 2.31 \ln\gamma$ for r = 1.

The reasons for the above two empirically observed relationships can be seen by expressing Equation (1) in its classical statistics form. The classical statistics approximation is valid for both charge carriers at optimum doping only for large values of β and η_G (near the upper right corners of the families of curves of Figures 10 and 11). For

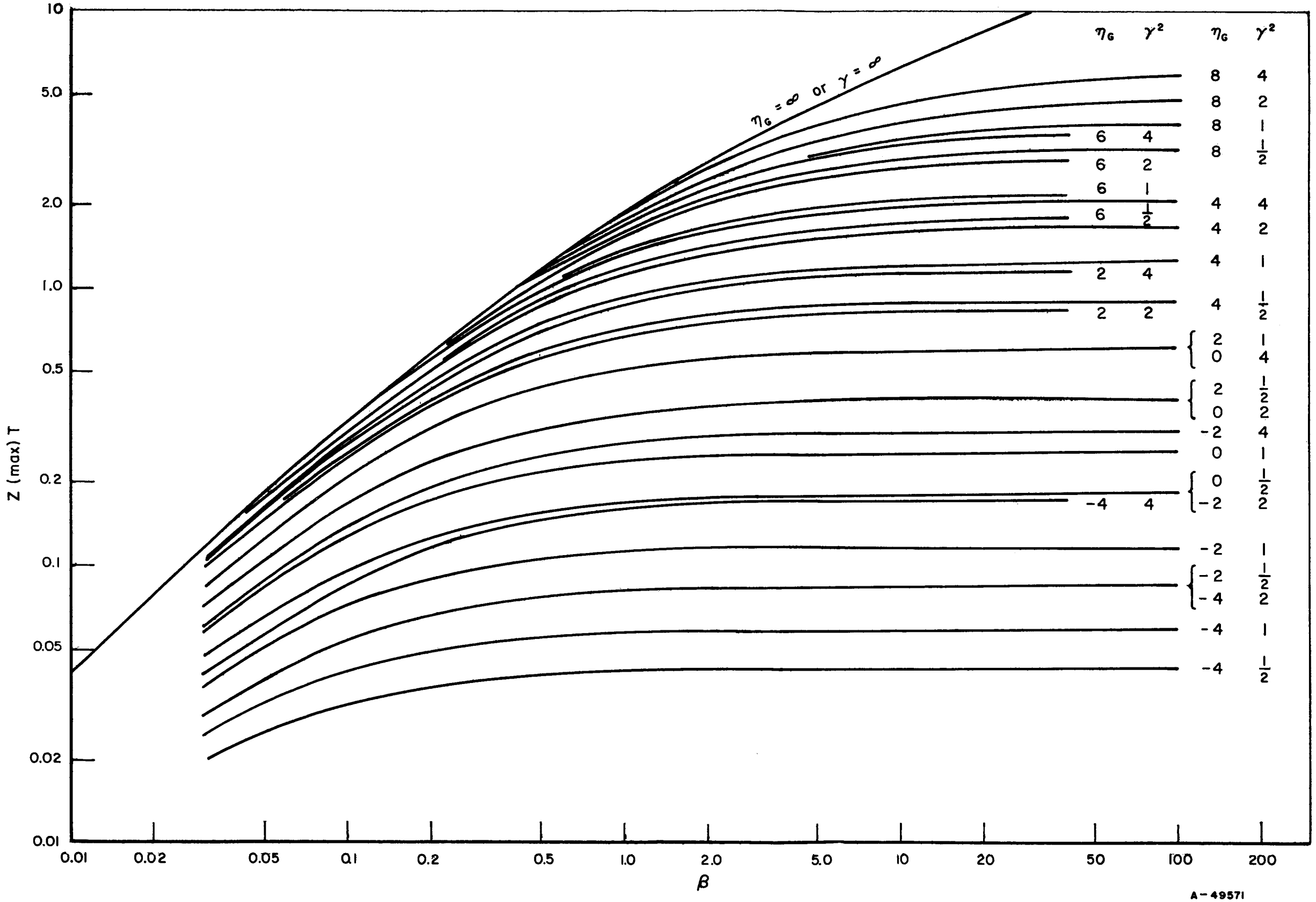

FIGURE 10. Z(max)T AS A FUNCTION OF β FOR r = 0 AND FOR VARIOUS VALUES FOR η_G AND γ

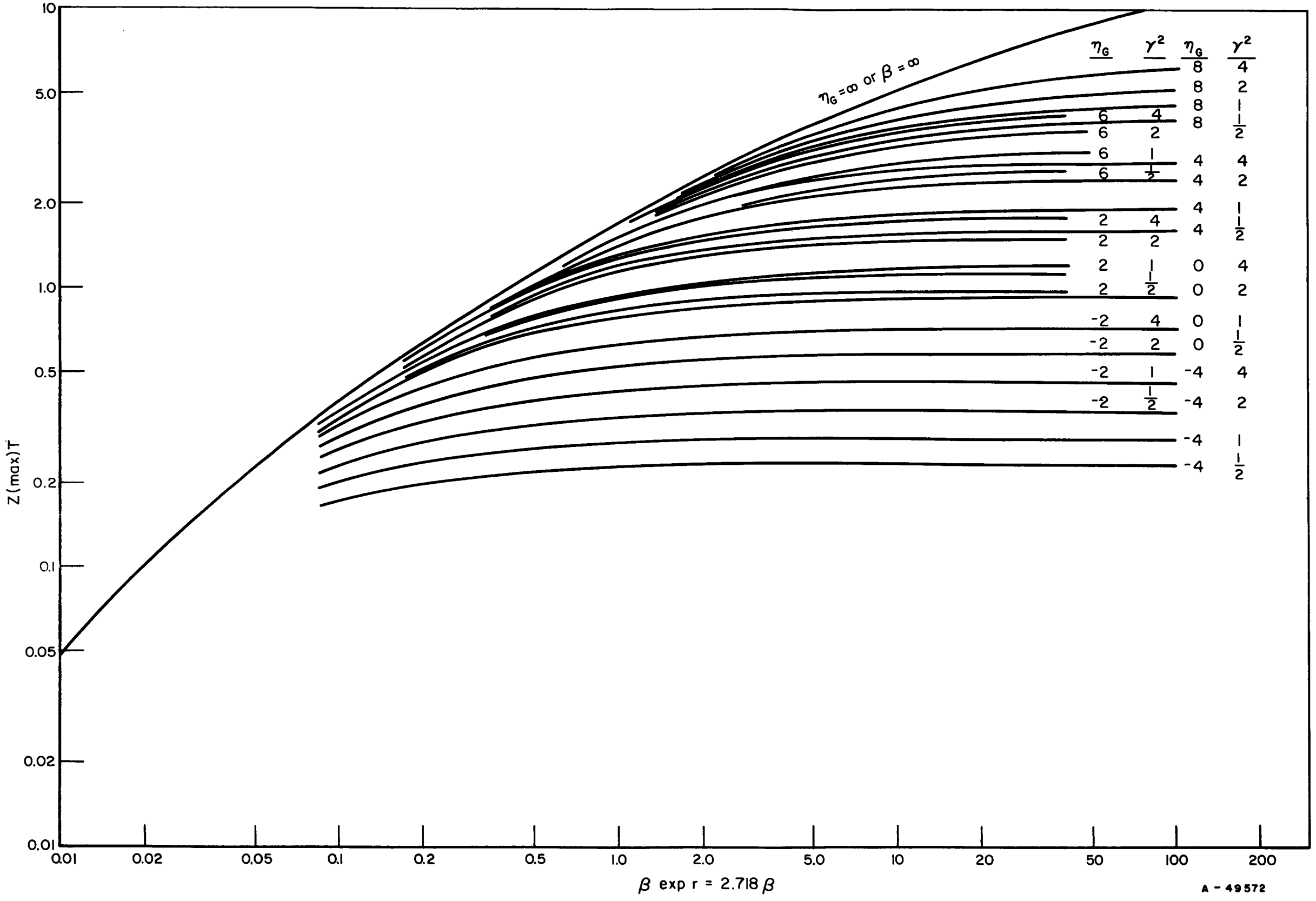

FIGURE 11. Z(max)T AS A FUNCTION OF β exp r FOR r = 1 AND FOR VARIOUS VALUES OF η_G AND γ

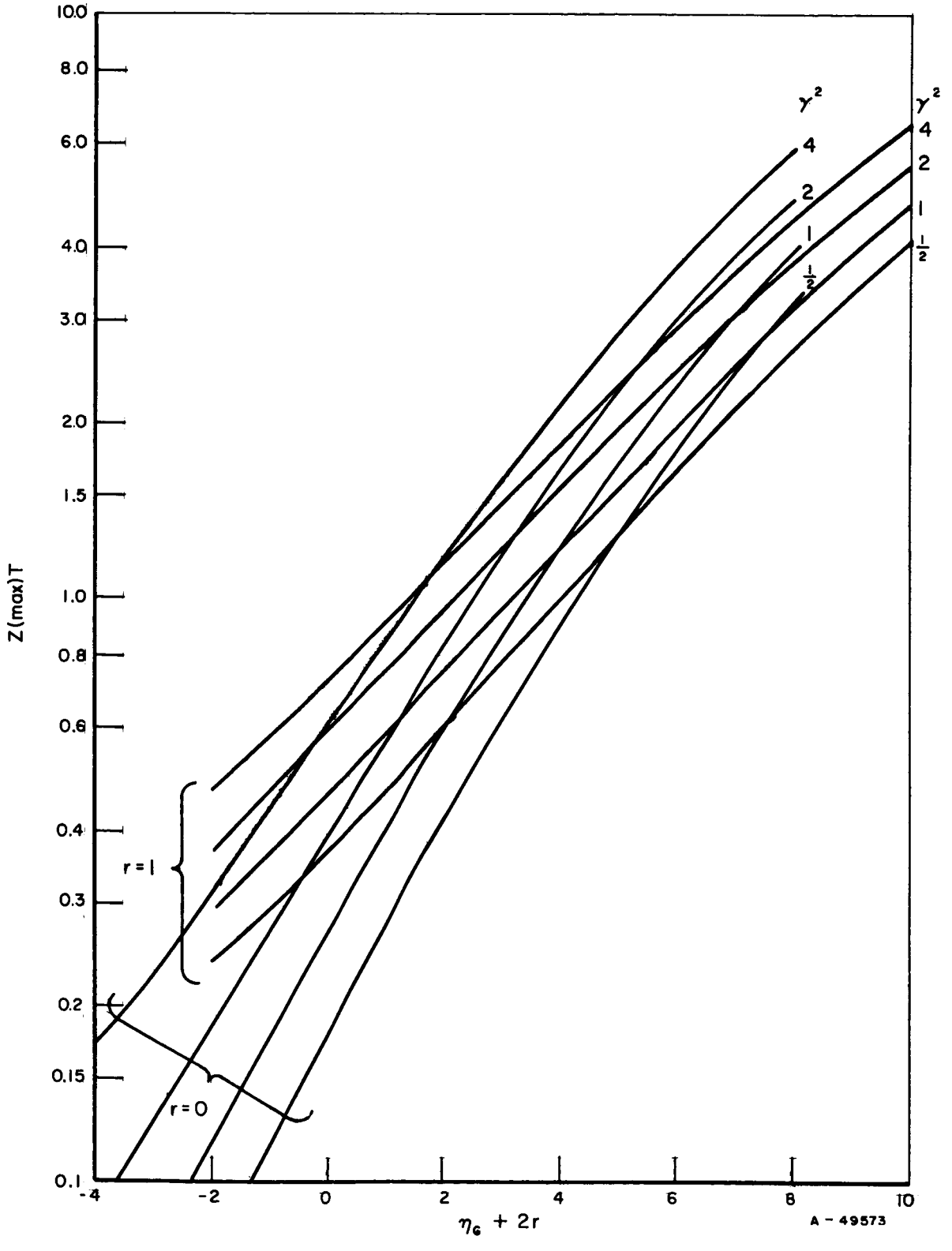

FIGURE 12. Z(max)T AS A FUNCTION OF $\eta_G + 2r$ AND γ FOR $\beta = \infty$

classical statistics, ($\eta_e \ll 0$), Equations (2), (3), and (4) become $A_e = -(r + 2 - \eta_e)$, $B_e = \exp \eta_e$, and $L_e = r + 2$, respectively, with corresponding expressions for A_h, B_h, and L_h. We then have

$$ZT\begin{pmatrix}\eta_e \ll 0\\ \eta_h \ll 0\end{pmatrix} = \frac{[-(r+2+\eta_G/2)\tanh(\eta_e+\ln\gamma+\eta_G/2)+\eta_e+\eta_G/2]^2}{(2\beta)^{-1}\exp(\eta_G/2+\ln\gamma)\,\mathrm{sech}(\eta_e+\ln\gamma+\eta_G/2)+(r+2)+(r+2+\eta_G/2)^2\,\mathrm{sech}^2(\eta_e+\ln\gamma+\eta_G/2)} \quad \cdot (9)$$

If only the combinations $r+2+\eta_G/2$ and $\ln\gamma+\eta_G/2$ appeared in Equation (9), then Z(max)T would be a function of η_G+2r and of $\eta_G+2\ln\gamma$ in the classical statistics limit. However, both the quantities $\eta_G/2$ and $r+2$ are seen to occur also separately in Equation (9). This prevents the empirical relationship mentioned above from being precise.

$(ZT)_{max}$ Considerations. The $(ZT)_{max}$ considerations are facilitated by replotting Figures 10 and 11 in the form of Figures 13 and 14, respectively, showing contours of constant values of Z(max)T on a grid of $\beta \exp r$ versus $\eta_G + 2.89 \ln\gamma$ for $r = 0$ and versus $\eta_G + 2.31 \ln\gamma$ for $r = 1$. These constant Z(max)T curves are the solid-line curves in Figures 13 and 14.

The broken-line curves on Figure 13 represent the loci of points of the values of $\beta + 2.89 \ln\gamma$ for hypothetical materials as the temperature is changed and the doping adjusted to optimum at each temperature. For these broken-line curves it is assumed that m_d is independent of T, that μ_{ce} varies as $T^{-3/2}$, and that K_L varies as T^{-1}. Consequently, β varies as T^2, in accordance with Equations (5) and (6). It is also assumed that η_G varies as T^{-1}, corresponding to neglect of the temperature dependence of the energy gap, and that $\gamma = 1$ at any temperature.

The value of $(ZT)_{max}$ for any given material corresponds to the point where the broken-line curve for that material becomes tangent to one of the curves of Z(max)T = constant. Thus, a hypothetical material with, say, room-temperature values of $\beta = 0.16$, $\gamma = 1$, $\eta_G = 16$ and Z(max)T = 0.50 (Point A on Figure 13) would be predicted to have a value of $(ZT)_{max}$ of slightly over 1.40 at $\beta = 0.90$ and $\eta_G = 6.7$, at a temperature of $T = 300\ (2.45) = 730°K$ (Point B on Figure 13). It is assumed, of course, that no phase changes occur in the material when raising the temperature from that corresponding to Point A to that corresponding to Point B. It is also emphasized that the Z(max)T values corresponding to both Points A and B are the ZT values at optimum doping and not necessarily the actual ZT values of the same specimen of the material at these respective temperatures, since the optimum concentration of impurity doping at Point B is not necessarily the same as that of Point A. These curves enable us to predict the potentialities of a given material at any temperature, subject to the limitations of phase stability and ability to obtain the proper dopant concentration at that temperature.

Consider the third broken-line curve from the left, the one that passes through the point $\eta_G + 2.89 \ln\gamma = 10$, $\beta = 0.01$ at the bottom of the figure. This curve is closely tangent to the Z(max)T = 0.35 solid curve over the range from about $\eta_G = 1.5$, $\beta = 0.4$ to about $\eta_G = 0.5$, $\beta = 3.6$. This represents a 3 to 1 range in T. On the other hand the broken-line curve on which Points A and B lie is tangent to the Z(max)T = 1.4 curve from about $\eta_G = 6.0$ to about $\eta_G = 7.2$, which is only about a 1.2 to 1 range in T. It is seen that the higher the value of $(ZT)_{max}$, the smaller is the temperature range over which $Z(max)T = (ZT)_{max}$. This observation is of evident technical importance in the design

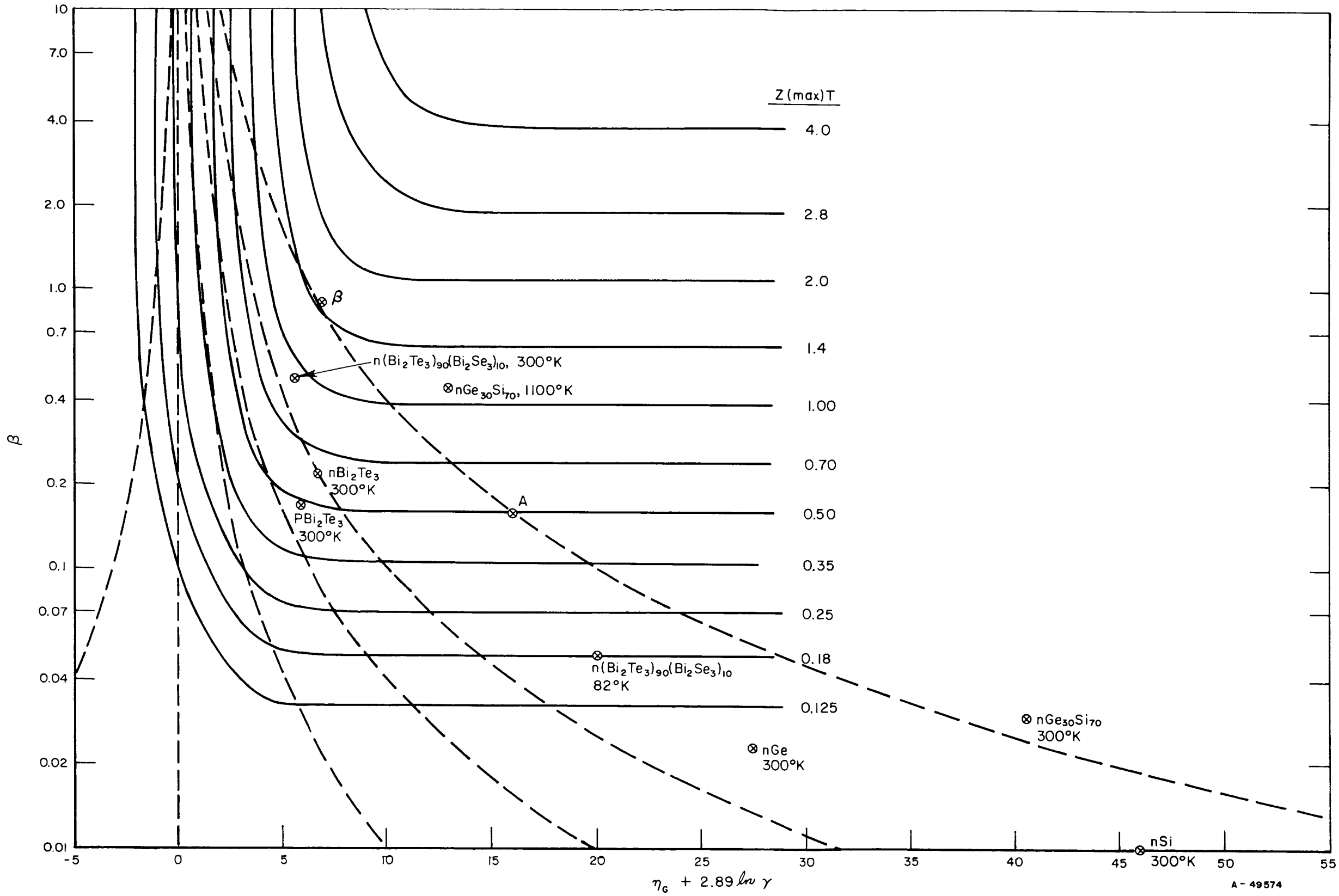

FIGURE 13. CONTOUR PLOT OF CONSTANT Z(max)T FOR r = 0

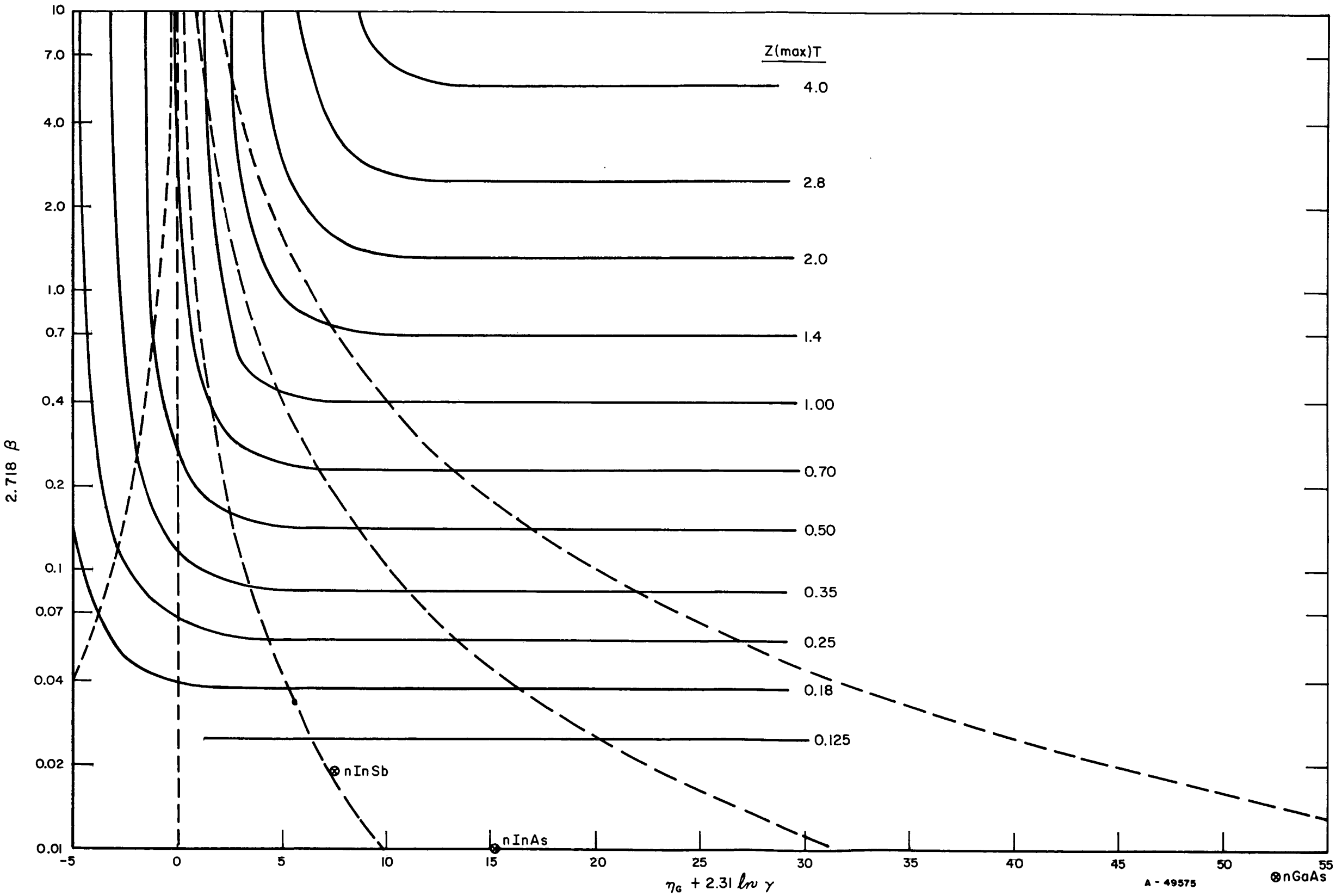

FIGURE 14. CONTOUR PLOT OF CONSTANT Z(max)T FOR r = 1

of thermocouple legs with the possibly improved materials of the future, since the better the material the more restricted is the temperature range over which it could operate at $(ZT)_{max}$. The fact that the critical temperature range over which $Z(max)T = (ZT)_{max}$ becomes more restricted for the better materials may be one of the reasons why it has been so difficult to find improved materials.

As long as β increases monotonically with temperature, the broken-line curves of all materials on Figures 13 and 14 must approach the $\eta_G = 0$ vertical line asymptotically as the temperature increases indefinitely. For the poorer materials this asymptotic approach parallels one of the Z(max)T = constant curves over a wide temperature range. However, for the better materials the asymptotic approach of the broken lines to $\eta_G = 0$ necessitates that they can become tangent to a Z(max)T = constant curve only over the small temperature interval that covers the high-curvature transition region between β-sensitive and η_G-sensitive Z(max)T behavior.

It is of interest to note that the two-band theory predicts that Z(max)T would approach a finite value as the temperature is increased indefinitely ($\eta_G \rightarrow 0$), that is, the high-temperature limit of Z(max) should vary as T^{-1}. The ordinates on Figure 12 for $\eta_G = 0$ show that the limiting high-temperature values of Z(max)T for r = 0 are 0.61, 0.40, 0.26, and 0.18 for $\gamma^2 = 4$, 2, 1, and 1/2, respectively, and for r = 1 are 1.15, 0.95, 0.74, 0.60 for $\gamma^2 = 4$, 2, 1, and 1/2, respectively. The optimum Fermi energies corresponding to these values of Z(max)T in the high-temperature limit range from about 1 to about 4 kT above the band edge, depending upon the values of r and γ. Since the density of states increases as $T^{3/2}$, the concentration of impurity doping must also be increased as $T^{3/2}$ in order to maintain the optimum degree of Fermi degeneracy as the temperature is increased. It seems that the only practical way advantage might be taken of these high-temperature Z(max)T values would be for optimum Fermi level to correspond to intrinsic or nearly intrinsic material. This is perfectly possible, as pointed out in Reference (2). For example, if $\eta_e(opt) = 1.0$, $\eta_h = -1.0$ for $\eta_G = 0$, and this would correspond to intrinsic material if $m_e/m_h = [F_{1/2}(-1)/F_{1/2}(+1)]^{2/3} = 0.35$.* The requirement that β increase monotonically with temperature may also be violated as additional mechanisms of heat transport become important at higher temperature. For example, if radiative heat transport becomes important enough for K_L to begin to increase at least in direct proportion to T, β would begin to decrease with increasing temperature.

Figures 13 and 14 could be used to predict the temperature behavior of Z(max)T and to find the value of $(ZT)_{max}$ for any real material (the values for which might not necessarily run parallel to the family of broken lines as the temperature is changed). In order to trace the locus of points of any real material on these figures it is necessary to know how μ_{ce} and μ_{ce}/μ_{ch} vary with temperature, the former for use in determining the temperature variation of σ_{oe} and the latter for determining the temperature variation of γ. The variations of m_{de} and m_{de}/m_{dh} with temperature at the optimum doping level would likewise be needed for the same purposes, if one or both energy bands are nonparabolic. The variation of energy gap with temperature must also be known to obtain the correct temperature variation of η_G. If the temperature range in question covers a transition region of mixed scattering mechanisms, say acoustical- and optical-mode scattering, some kind of average value of $(ZT)_{max}$ must be estimated from Figures 13 and 14 pending the extension of this development to the case of mixed scattering. Likewise, the possible activation of additional energy bands with increase in temperature can be treated only by the approximate analytical methods to be described later, pending

*The value of m_e/m_h is not directly related to γ^2, since the latter equals $m_e^{3/2}\mu_e/m_h^{3/2}\mu_h$.

calculations of Z(max)T for multiband cases. The basic theory for the thermoelectric ZT of multiband materials has been developed but not yet applied to make these calculations.[7]

Material Studies

Preliminary Considerations. In the attempt to establish more useful criteria for the selection and development of improved thermoelectric materials, it was felt advisable to compute and tabulate the values of the basic two-band model parameters discussed above for all of the semiconductors and semimetals for which the necessary information could be found in the literature. Any correlations that may exist between the energy band model and other models of semiconductor behavior pertinent to thermoelectric quality as measured by the figure of merit would be of significance only in terms of correlations with various combinations of these basic parameters. Of course, if some measure of a single parameter of another model correlated with the same functional combination of the basic parameters that determines the values of either Z(max)T at a given temperature or $(ZT)_{max}$ at optimum temperature, this parameter would be of much greater value as a selection criterion than the individual basic parameters of the two-band model, which are β, γ, η_G, and r. This possibility is a very unlikely one, however.

The information needed for computing the values of the basic parameters of the two-band model are the numbers of equivalent energy extrema of the conduction and of the valence band, the effective masses and mobilities of the charge carriers in these valleys, the lattice component of the thermal conductivity, the value of the forbidden energy gap between the conduction and valence bands, and the scattering parameters for the charge carriers. It is understandable that room temperature (T = 300°K) would be the only common temperature at which such data would be available for a wide variety of materials. Consequently, only the room-temperature values of the various parameters are computed and tabulated. As pointed out previously, however, the primary interest would usually be in comparing the thermoelectric potentialities of materials at their optimum temperatures, whatever these might be, rather than at a single, fixed temperature. To aid in using Figures 13 and 14 to estimate $(ZT)_{max}$ for each material, the temperature dependences of the charge carrier mobilities are also tabulated, if available. The room-temperature values of the energy gap are tabulated, whenever available, and the temperature dependences of the energy gaps are ignored as having only a second-order effect on the variation of η_G with temperature for most materials over the usual ranges of temperature of interest. Other neglected factors, such as the effects of nonparabolicity of the band structure on the variation of effective mass and mobility with temperature and carrier concentration and the activation of additional energy bands with increasing temperature, may lead to greater errors in the estimate of $(ZT)_{max}$ than neglect of the temperature dependence of the energy gap. It is understandably not feasible in such a compilation covering a large number of materials to take everything into account. In computing the temperature variation of β for the purpose of determining $(ZT)_{max}$, for example, it was simply assumed that K_L varies as T^{-1} in the neighborhood of room temperature. However, more accurate analyses can always be made for specific materials using the measured temperature variation of the various parameters.

The electron energy band structure of semiconductors consists, in general, of a multiplicity of allowed energy bands. The validity of the two-band model rests on the

assumption that we need to consider only the highest filled energy band (the valence band) and the lowest lying conduction band above it. The rule that has been followed in calculating the parameters for the equivalent two-band model is to ignore all energy bands whose extrema are 4 kT (at room temperature) or more removed from the primary conduction or valence bands. If another band extremum is spaced by less than about 1.5 kT (at room temperature) from the extremum of its counterpart primary band, the energy separation is neglected and the values of $m_d^{3/2}\mu$ for the two bands are added together in order to obtain the value of σ_o. The intermediate situation, where the energy spacing is between 1.5 and 4 kT, is treated by adding in some fraction of the $m_d^{3/2}\mu$ value for the more remote band, depending on the amount of energy separation. Possible band interactions and effects of interband scattering of charge carriers are not considered.

The above rules for computing equivalent two-band parameters for multiband cases are based on the results of Z(max)T computations made for extrinsic semiconductors with either two conduction bands or two valence bands.[8] The expression for ZT for the two-like-band case would be identical with Equation (1) if the subscript e's and subscript h's were replaced by subscript 1's and subscript 2's, respectively, enumerating the two individual bands. A_1 and A_2 would be of the same algebraic sign rather than of opposite signs.

In some cases, such as for the two degenerate valence bands of the III-V compounds, the values of the effective masses are known for the two bands separately but only a single value is given in the literature for the mobility of the holes. We need to know the partial mobilities of the holes in the individual bands since the equivalent single-band value of σ_o is proportional to $m_1^{3/2}\mu_1 + m_2^{3/2}\mu_2$. If the given single mobility value, $\overline{\mu}_{12}$, is based on a Hall mobility measurement it is readily shown that

$$m_1^{3/2}\mu_1 + m_2^{3/2}\mu_2 = (m_1 m_2)^{1/2}(m_1^{1/2} + m_2^{1/2})\overline{\mu}_{12} \quad . \tag{10}$$

In deriving Equation (10) it is assumed that the two partial mobilities are inversely proportional to the respective effective masses (same relaxation time for the charge carriers in the two bands) and that the carrier concentrations in the individual energy bands are directly proportional to the 3/2-power of the effective masses (same energy extremum for the two bands).

Results. Tables 6 through 14 list the room-temperature values of the pertinent constants and the computed values of β, γ, and η_G for the various elemental and binary compound semiconductors for which sufficient information was available from the literature. Blanks in the list do not necessarily imply that the corresponding information is not available; it may have not yet been compiled. These tabulations will be revised and extended from time to time as more or better data become available. They will also be extended, if it is seen that useful information can be obtained by so doing, to cover various alloys of the compounds listed and also ternary and higher order compounds.

All entries in the tables are in the commonly employed physical units of cm^2/volt sec for μ, ohm^{-1}-cm^{-1} for σ_o, watts/cm°C for K, and electron volts for E_G. All other quantities are dimensionless, including the effective masses, which are expressed in the conventional manner in terms of ratios of the free electron mass. The quantity N denotes the number of equivalent band extrema and m_1, m_2, and m_3 are the three principal effective masses for each extremum. For cubic crystals with extrema on the (100) or (111) axes, for which symmetry dictates the equality of the two transverse masses, the

TABLE 6. GROUP IV SEMICONDUCTORS

Material	N	$m_{\|\|}$	$m_{\perp}$	$Nm_d^{3/2}$	μ	$\frac{-d \ln \mu}{d \ln T}$	σ_o	$\sigma_o e^r$	K_L	β	γ	E_G, Δ	η_G	References
n Ge	4	1.588	0.0815	0.410	3,800	1.66	6240	6240	0.61	0.023	2.0	0.66	25.4	14 through 21
p_h	1	0.28		0.148	1,800	2.38	1070					0		
p_l	1	0.044		0.0092	13,500		500					0.28		
p_{so}							1570	1570		0.0057				
n Si	6	0.90	0.192	1.100	1,450	2.6	6380	6380	1.41	0.010	2.7	1.12	43.0	17,21,22,23
p_h	1	0.49		0.343	500	2.3	690					0		
p_l	1	0.16		0.064	1,500		100					0.044		
p_{so}	1	0.245		0.121	1,000		120							
							910	910		0.0014				
n C (diamond)		0.25-0.6			900-3900	1.5			5.7			5.6	215	24,25,26
p		0.25-0.6			1200-4800	1.5-2.8								
n Sn (gray)	4	1.6	0.6	0.304	≈2,000		≈2600					≈0	0	27
	1	0.03		0.0052								≈0		
p	1	0.35		0.207	≈1,000		≈830							
n β SiC		0.7			20-100							1.90		28
p		1.2			10-25									

TABLE 7. III-V COMPOUNDS

Material	N	m	$m^{3/2}$	μ	$\frac{-d \ln \mu}{d \ln T}$	σ_o	$r = l_r$ $\sigma_o e$	K_L	βe^r	γ	E_G	η_G	References
n In Sb	1	0.014	0.00166	78,000	1.68	520	1420	0.17	0.019	1.58	0.17	6.5	21,29,30,31
p_h	1	0.40	0.0692	750	2.1	210	570		0.0075				
p_l	1	0.02											
n In As	1	0.022	0.00326	33,000	1.5	430	1170	0.27	0.0096	1.69	0.36	14	
p_h	1	0.41	0.081	460	>2	150	410		0.0034				
p_l	1	0.025											
n In P	1	0.067	0.0174	4,600	2	320	870	0.67	0.0029	1.88	1.29	50	
p_h	1	0.4	0.15	150	2.4	90	245		0.00081				
p_l	1	0.07											
n Ga Sb	1	0.047	0.0102	low 4,000	1.5	low 165	low 450	0.38		0.63-?	0.67	26	
p_h	1	0.23	0.073	1,400	1.5	410	1120						
p_l	1	0.05-?											
n Ga As	1	0.068	0.0177	8,800	1	620	1690	0.46	0.0082	1.26	1.35	52	
p_h	1	0.5	0.247	400	2.1	390	1060		0.0051				
p_l	1	0.07-?											
n_h Ga P	3	0.35	0.206	300		250	680	~1.09	~0.0014	1.31			
n_l	1	0.12									2.25	87	
p_h	1	0.4	0.214	170		145	395		0.00081				
p_l	1	0.12-?											
n_h Al Sb	3	0.39	0.243	200-450		~200	540	0.46	0.0026	0.71	1.62	62	
n_l	1	0.09											
p	1	0.4	0.177	200-450		~390	1060		0.0051				

TABLE 8. II-VI COMPOUNDS

Material	m	$m^{3/2}$	μ	$\frac{-d \ln \mu}{d \ln T}$	σ_o	$\sigma_o e^r$	K_L	βe^r	γ	E_G	η_G	References
n ZnS	~0.4	0.253	100		100		0.27	0.00083		3.6	140	32
p												
n ZnSe	~0.1	0.0316	260		32		0.13	0.00055		2.6	100	
p	~0.6											
n ZnTe							0.11			2.2	85	
p			425									
n CdS	0.2	0.0895	295		105				1.90	2.4	92	
p	0.8	0.715	10		29							
n CdSe			550	1.0						1.7	65	
p												
n CdTe	0.14	0.0523	800		125				1.18	1.44	55	31,32,33
p	0.37	0.225	100		90							
n HgS										2.0	77	
p												
n HgSe	0.045	0.0095	7,000	2	270					0.2	7.7	
p												
n HgTe	0.030	0.0052	22,000		460	1250	0.027	0.103		0.02	0.77	31,34
p			1,600									
n ZnO	0.27	0.140	180	1.5	100		0.006	0.037		3.2	12	35
p												
n CdO	0.1	0.032	120		15		0.007	0.0048		2.5	10	
p												
n SrS										4.1	16	
p												

TABLE 9. IB-VI COMPOUNDS

Material	N	m_1	m_2	m_3	$Nm_d^{3/2}$	μ	$\frac{-d \ln \mu}{d \ln T}$	$\sigma_o e^r$	K_L	β	γ	E_G	η_G	References
n Ag_2S														
p														
n $Ag_2Se(\beta)$					0.113	1860		840	0.002	0.94	1.75	0.034	1.3	36
p														
n Ag_2Te														
p														
n Cu_2S														
p														
n Cn_2Se														
p														
n Cu_2Te														
p														

TABLE 10. IV-VI COMPOUNDS

Material	N	$m_{\|\|}$	$m_\perp$	$Nm_d^{3/2}$	μ	$\frac{-d \ln \mu}{d \ln T}$	σ_o	$\sigma_o e^r$	K_L	β	γ	E_G	η_G	References
n Pb S	6 (110)	0.16		0.064	550		140		~0.03	~0.010		0.37	14	35,37,38
p	12				600	2.2								
n Pb Se	1 (000)	~0.3		0.164	1020		670		0.017	0.088		0.26	10	
p	1 (000)				930	2.2								
n Pb Te	1 (000)													
n	4 (111)	0.11	0.025	0.033	1620		215			0.022	1.28	0.29		35,37,38,39
p	1 (000)	0.12		0.117	750				0.022				11	
p	4 (111)	0.26	0.04			2.2	350			0.036				

TABLE 11. V-VI COMPOUNDS

Material	N	m_1	m_2	m_3	$Nm_d^{3/2}$	μ	$\frac{-d \ln \mu}{d \ln T}$	σ_o	$\sigma_o e^r$	K_L	β	γ	E_G	η_G	References
n As_2Te_3			— 0.36 —		0.60	170		410		0.025	0.037	1.34	1.00	38	35
p			— 0.50 —		0.71	80		230			0.021				
n Sb_2Se_3						15-?							1.20	46	
p						45-?									
n Sb_2Te_3			— 0.3 —		0.55					0.055					
p			— 0.34 —		0.58	280		650			0.026				
n Bi_2Se_3						600				0.024			0.35	13	
p															
n Bi_2Te_3	6		— 0.45 —		0.30	1330	1.68	1600	1600	0.016	0.22	1.15	0.16	6.2	40-42
p	6	0.0505	0.207	0.38	0.38	790	1.98	1200	1200		0.17				

TABLE 12. II-V COMPOUNDS

Material	$m_{\parallel}$	$m_{\perp}$	$Nm_d^{3/2}$	μ	$\frac{-d \ln \mu}{d \ln T}$	σ_o	$\sigma_o e^r$	K_L	β	γ	E_G	η_G	References
n ZnSb	0.175	0.146	0.061	10				0.014			0.56	22	31, 35
p				340									
n CdSb	0.140	0.159	0.059	~300				0.01			0.465	18	
p	0.1-0.2			~1100									
n Zn_3As_2											0.93	36	
p				10	1.1								
n Cd_3As_2	0.10			1500	0.88			0.11			0.13	5.0	
p													
n Mg_3Sb_2											0.82	32	
p				82									
n $CdAs_2$	0.150	0.580									1.13	43	43
p	0.094	0.346											

TABLE 13. MISCELLANEOUS ELEMENTAL SEMICONDUCTORS

Material	N	m_1	m_2	m_3	$Nm_d^{3/2}$	μ	$\frac{-d \ln \mu}{d \ln T}$	σ_o	σ_{oe^r}	K_L	βe^r	γ	E_G	η_G	References
n C-graphite	3	0.031	0.031	0.36	0.0557	12,500	1.2	2780	2780	2-4	~0.0021	0.71	-0.035	-1.35	44,45
p ($\perp$c-axis)	3	0.066	0.066	0.77	0.1114	16,000	1.2	5560	5560		~0.0041				
n Te	3	0.374	0.324	0.324	0.594	910		2160		0.023 (IIC)			0.34	13	35
p	3	0.123	0.085	0.044	0.0642	570		150							
n Sb															
p															
n Bi	3														
p Bi															
n Se										0.02					
p															

TABLE 14. ISOELECTRONIC SERIES

Material	% Ion	$1/2 (A_1 + A_2)$	A_1/A_2	K_L	μ_e	σ_{oe}	β_e
GaP	6	50.5	2.24	1.09	300	250	0.00051
ZnS	26	48.8	2.10	0.27	100	100	0.00083
CuCl	30	49.5	1.80	~0.008			
Ge	0	72.6	1.00	0.61	3,800	6240	0.023
GaAs	4	72.3	0.94	0.46	8,800	620	0.0030
ZnSe	19	72.1	0.82	0.13	260	32	0.00055
CuBr	22	71.8	0.80	0.011			
GaSb	2	95.8	0.57	0.38	low 4,000	low 165	
ZnTe	11	96.5	0.51	0.11			
CuI	15	95.3	0.50	0.017			
Sn-gray	0	118.7	1.00		~2,000		
InSb	2	118.3	0.95	0.17	78,000	520	0.0068
CdTe	15	120.0	0.89	0.063	800	125	0.0044
AgI	15	119.4	0.85	~0.004			

designations $m_\perp$ and $m_{||}$ are employed. The listing of a single mass value does not necessarily imply that the energy band in question has only a single extremum at the center of the Brillouin zone; only a total density-of-states mass value may be known for that particular material. The prefix n before the name of a compound designates that the constants pertinent to the conduction band are listed on that row. The prefix p refers to the valence band, with subscripts, ℓ, h, and so, designating light hole, heavy hole, and split-off bands. At T = 300°K and in terms of the above units, $\sigma_o = 4.00\ N m_d^{3/2} \mu$, and $\beta = 2.23 \times 10^{-6}\ \sigma_o / K_L$.

In the following sections some preliminary comments that seem to be significant will be made regarding some of the tabulated results. More complete discussions of the tabulations will be deferred until subsequent quarterly reports.

Group IV Semiconductors. Table 6 lists the data and results of the computations for the Group IV semiconductors of cubic symmetry, with the data for the best known semiconductors, silicon and germanium, forming the only complete set of information in this table. Some data for elemental semiconductors of noncubic symmetry are given in Table 13. A brief review of the energy-band structures of the Group IV semiconductors and of the other semiconductors for which the band structures are relatively well understood is given in Reference (9). The band structures of the specific materials of the thermoelectric interest are reviewed briefly in Reference (10).

The values of σ_o for electrons are about the same for germanium and silicon and represent by far the largest known values of σ_o for any semiconductors. As can be seen from Equations (5) and (6), σ_o combines all the factors in the material parameter β that are directly pertinent to the transport properties of the charge carriers. The values of σ_o for the electrons of gray tin and of graphite (for conduction in the plane perpendicular to the c-axis) are about the same and represent the second highest σ_o values for electrons for any semiconductors (see Table 13 for graphite). The σ_o value for the holes in graphite in the high-conductivity plane is almost the same as for that of the electrons in silicon or germanium. (The σ_o values for the holes in germanium and silicon are higher than those of most other materials, but are not unusually high.)

The superior characteristics of the conduction bands of germanium and silicon and of the valence band in graphite, as far as the charge carrier contribution to desirable thermoelectric properties are concerned, are the result of the multivalleyed structure with a high degree of mass anisotropy in each valley. As previously pointed out,[2,8] a large number of equivalent valleys plus a high mass anisotropy per valley contribute to a high value of σ_o. The degree of overall anisotropy of electrical conduction in the crystal seems to have little bearing on the matter, as can be seen by comparing graphite, which has the greatest degree of conduction anisotropy of any known material and silicon and germanium which exhibit isotropic conductivity. This is in accordance with theoretical expectations. As a matter of fact, it is demonstrated in Reference (8) that crystals with cubic symmetry may have a slight advantage in possessing higher σ_o values. The larger number of valleys permitted by cubic symmetry is shown to override slightly the possible advantage in an anisotropic crystal of being able to maximize σ_o by choice of the current direction with respect to the crystallographic axes. The degree of mass anisotropy per energy ellipsoid is assumed to be the same in the two cases.

The characteristic (β, $\eta_G + 2.89 \ln\gamma$) points for nGe and nSi at room temperature are plotted on Figure 13. The values of β, and consequently of Z(max)T, are low for

nGe and nSi at T = 300°K because of the high values of K_L, despite the high values of σ_o. From the positions of these characteristic points about midway between broken-line curves, it can be estimated how the values of Z(max)T for both nGe and nSi would increase with temperature, both reaching $(ZT)_{max}$ values of about 1.0 somewhere near their respective melting points. Actually, since the electron mobilities of germanium and silicon decrease more rapidly than $T^{-1.5}$, the locus of the characteristic points for nGe and nSi as the temperature is raised may well pass near or below the plotted points on Figure 13 for n and p Bi_2Te_3 at T = 300°K.

It is more instructive to consider one of the Ge-Si alloys for which high-temperature thermoelectric data are available. The room-temperature characteristic point for the $nGe_{30}Si_{70}$ alloy is also shown on Figure 13. The β-value for this point was computed from the information on the Seebeck coefficient, electrical conductivity, and thermal conductivity given in Reference (11). Despite the appreciably lower value of 1200 ohm^{-1}-cm^{-1} for σ_o for this alloy, β is greater than for either 100 percent silicon or germanium because of the much lower value of K_L for the alloy. The value of $\eta_G + 2.89 \ln\gamma$ for this alloy was chosen by using linear interpolation on the energy gap and on the value of γ between silicon and germanium.

The characteristic point for T = 1100°K for the same $Ge_{30}Si_{70}$ alloy is plotted on Figure 13, also based on actual data in Reference (11). It is seen that β increases at roughly the same rate with temperature as is represented by the broken lines ($\beta \propto T^2$). It is also seen that $(ZT)_{max}$ for this alloy would be just slightly over 1.40, at η_G corresponding to a temperature of about 1700°K, somewhat above the melting point. Measurements are reported in Reference (11) up to 1300°K. The actually measured value of ZT for this alloy at 1100°K is given in Reference (11) as 1.0, whereas the characteristic point in Figure 11 indicates a Z(max)T value of about 1.1. This shows that the particular specimen in question was not quite optimally doped for 1100°K. The extrinsic carrier concentration for this specimen was $1.5 \times 10^{20}/cm^3$; heavy doping is required because of the high values of m_d and T involved.

It is instructive to plot on the same figure the characteristic point for the $n(Bi_2Te_3)_{90}(Bi_2Se_3)_{10}$ alloy at T = 300°K, computed from the data on this material in Reference (3). This latter characteristic point has about the same value of β but a much lower value of $\eta_G + 2.89 \ln\gamma$ than for $nGe_{30}Si_{70}$ at T = 1100°K, indicating the superiority of the latter as a thermoelectric material. Hence, there is probably nothing particularly unique about the band structure, crystallography, or chemical bonding of Bi_2Te_3 to which its superior thermoelectric properties are attributable. It is a valuable material for thermoelectric cooling applications because its $(ZT)_{max}$ point occurs near room temperature. In $nGe_{30}Si_{70}$ with an entirely different structure, bonding, and crystallography we have a material whose thermoelectric properties are superior to those of the Bi_2Te_3 alloy at the optimum temperatures for both materials, at two to three times their respective Debye temperatures.[12] Also plotted on Figure 13 is the 82°K characteristic point for $n(Bi_2Te_3)_{90}(Bi_2Se_3)_{10}$ to show that its temperature dependence is "normal".

The III-V Compound Semiconductors. Table 7 lists the data and computations of $\beta \exp r$, γ, and η_G for the III-V compounds. The value of r = 1 has been chosen for computing $\sigma_o e^r$ and βe^r since, as pointed out by Ehrenreich,[13] the dominant scattering mechanism for electrons in the III-V compounds at room temperature is by the optical-mode lattice vibrations. This occurs despite the small degree of ionicity of these compounds because of the very small values of the electron effective masses. The value

r = 1 was chosen arbitrarily for the holes as well as for the electrons for all of the III-V compounds. Although various degrees of mixed scattering would probably give a better representation, the Z(max)T theory for mixed scattering has not yet been developed. It is to be noted that if σ_o exp r is computed from resistivity and Seebeck coefficient data on extrinsic III-V compounds by the procedure outlined in the previous quarterly report, values intermediate between those listed in Table 7 for σ_o and for σ_o exp r are obtained.

It is noteworthy that although the electron mobilities for the various III-V compounds range in value over almost three orders of magnitude, the values of σ_o vary over a range of only about 2 to 1 (exclusive of the abnormally low value of σ_o for nGaSb). (The highest experimental value of the electron mobility for this latter compound is abnormally low for its position in the series, perhaps because of too high a concentration of residual charge carrier scattering centers that cannot yet be eliminated in preparation.) Despite the much higher electron mobilities of the III-V compounds (excluding GaP and AlSb whose lowest lying conduction band minima consist of three 100 valleys), the values of σ_o for the III-V compounds are an order of magnitude lower than those for silicon and germanium. Conduction bands of spherical symmetry (N = 1) with small effective masses result in low values of σ_o. (The values of σ_o for the valence bands of the III-V compounds are also low since these are also k = 0 extrema and the presence of the light-hole bands does not contribute much to the value of σ_o for the holes.) The value of the charge carrier mobility by itself is thus seen to be a poor criterion for the preselection of potential thermoelectric materials.

It is to be noted that GaAs has the highest value of σ_o of the n-type III-V compounds. InSb, with an order of magnitude higher mobility than that of GaAs, is only a close second in its σ_o value. Hence, even ranking the thermoelectric qualities of the III-V compounds among themselves in accordance with mobility is seen to be meaningless.

It is evident that InSb is the best thermoelectric material of all of the III-V compounds at room temperature only because of its distinctly lower value of K_L. In terms of $(ZT)_{max}$ at optimum temperature, however, it is clearly the worst one because of its small band gap. This can be seen from the characteristic point plots of nInSb, nInAs, and nGaAs on Figure 14. Comparison of Figures 13 and 14 shows that nGaAs is only slightly inferior to nSi in thermoelectric properties at room temperature. It would be instructive to consider the thermoelectric properties of GaAs or of a suitable alloy of GaAs with another III-V compound at elevated temperatures.

Discussion of Tables 8 through 14 concerned with other classes of compounds will be deferred until a later report. They are included here for reference.

ANTICIPATED WORK

Work plans for the next period include

(1) Preparation and evaluation of n- and p-type $Bi_{86}Sb_{14}$ alloys containing less than 1.8 atomic percent tellurium and 1.9 atomic percent tin, respectively

(2) If time permits, studies of the effect of inhomogeneity and composition on thermoelectric properties of Bi-Sb alloys

(3) Studies of the effect of composition on the electrical properties of Ag-Sb-Te alloys

(4) Studies of the effect of doping on the thermoelectric properties of $AgSbSe_2$

(5) Efforts to prepare homogeneous $AgFeTe_2$ and $AgFeSe_2$

(6) If time permits, preparation of Ag-Sb-Se-Te alloys

(7) Theoretical investigation to include:

(a) Some computations of the thermoelectric figure of merit using a three-band model in order to verify or modify the predicted thermoelectric behaviors obtained by using an approximate two-band model on the many materials characterized by substantial carrier concentrations in at least three energy bands.

(b) Some computations of the thermoelectric figure of merit as a function of impurity doping and temperature for cases of mixed scattering mechanisms for the charge carriers.

(c) Improvement and extension of the tabulated values of the basic thermoelectric parameters for the various known semiconductors, to include also alloys and ternary and higher order compounds for which the necessary data are available. Theoretical predictions based on electron energy band models concerning criteria for improved thermoelectric materials would be checked against available data. The existence of these tabulations would also facilitate the verification of proposed criteria based on other physical or chemical models.

The data upon which this report is based are recorded in Battelle Laboratory Record Books Nos. 21561, pp 1-91, and 21590, pp 1-44.

REFERENCES

(1) Simon, R., "Maximum Figure of Merit of Thermoelectric Materials", Advanced Energy Conversion, 1, 81 (1961).

(2) Simon, R., J. Appl. Phys., 33, 1830 (1962).

(3) Bate, R. T., "Technical Report No. 3 on Thermoelectric Properties of Bi_2Te_3-Bi_2Se_3 Alloys" to ONR (1960). Contract Nonr-2316(00) NR 017-434.

(4) Brown, D. M., and Heumann, F. K., J. Appl. Phys., 35, 1947 (1964).

(5) Lockheed Aircraft Corp., Interim Engineering Report No. 3, March, 1962.

(6) Abeles, B., and Meiboom, S., Phys. Rev., 101, 544 (1956).

(7) Simon, R., Solid-State Electronics, 7, 397 (1964).

(8) Simon, R., unpublished.

(9) Long, D., J. Appl. Phys., 33, 1682 (1962).

(10) Ilisavskii, Yu. V., p 10 in Thermoelectric Properties of Semiconductors, edited by V. A. Kutasov. Proceedings of First and Second Conferences on Thermoelectricity. Translation by Consultants Bureau, New York (1964).

(11) Dismukes, J. P., Ekstrom, L., Steigmeier, E. F., Kudman, I., and Beers, D. S., J. Appl. Phys., 35, 2899 (1964).

(12) Gul'tyaev, P. V., and Petrov, A. V., Sov. Phys. - Solid State, 1, 330 (1959).

(13) Ehrenreich, H., J. Appl. Phys., 32, 2155 (1961).

(14) Levinger, B., and Frankl, D., J. Phys. Chem. Solids, 20, 281 (1960).

(15) Price, M. B., Phys. Rev., 92, 681 (1953), and 93, 1204 (1954).

(16) McCarthy, K. A., and Ballard, S. S., Phys. Rev., 99, 1104 (1955).

(17) Dexter, R. N., Zeiger, H. J., and Lax, B., Phys. Rev., 104, 637 (1956).

(18) Dresselhaus, G., Kip, A. F., and Kittel, C., Phys. Rev., 95, 568 (1954), and 98, 368 (1955).

(19) Willardson, R. K., Harman, T. C., and Beer, A. C., Phys. Rev., 96, 1512 (1954).

(20) Macfarlane, G. E., McLean, T. P., Quan, J. E., and Roberts, V., Phys. Rev., 108, 1377 (1957), and 111, 1245 (1958).

(21) Stegmeier, E. F., and Kudman, I., Phys. Rev., 132, 508 (1963).

(22) Rauch, C. J., Stickler, J. J., Zeiger, H. J., and Heller, G. S., Phys. Rev. Letters, 4, 64 (1960).

(23) Morin, F. J., and Maita, J. P., Phys. Rev., 96, 28 (1954).

(24) Robertson, R., Fox, J. J., and Martin, A. E., Phil. Trans., A232, 463 (1934).

(25) Redfield, A. G., Phys. Rev., 94, 526 (1954).

(26) Mitchell, E. J. W., J. Phys. Chem. Solids, 8, 444 (1958).

(27) Groves, S. H., ONR Technical Report No. HP-10 (Dec. 1963) NR-017-308. Contract No. Nonr-1866(10).

(28) O'Connor, J. R., and Smiltens, J., Ed., SiC, A High Temperature Semiconductor, Pergamon Press (1960).

(29) Hilsum, C., and Rose-Innes, A. C., Semiconducting III-V Compounds, Pergamon Press (1961).

(30) Hilsum, C., "Band Structure, Effective Charge and Scattering Mechanisms in III-V Compounds", paper presented at Paris Conference on Semiconductors (1964).

(31) Bube, R. H., Photoconductivity of Solids, John Wiley (1960).

(32) Hamilton, P. W., Advances in IV-V and II-VI Compounds, Semiconductor Progress and Solid State Technology, (June 1964), p 15.

(33) Froger, F. A., and deNobel, D., J. Electronics, 1, 190 (1955).

(34) Harman, T. C., et al, J. Phys. Chem. Solids, 7, 228 (1958).

(35) C. Beroit de la Guillaume, et al, Selected Constants Relative to Semiconductors, Ed. by P. Aigrain and M. Balkanski, Pergamon Press (1961).

(36) Simon, R., Bourke, R. C., and Lougher, E. H., Advanced Energy Conversion, 3, 481 (1963).

(37) Scanlon, W. W., Advances in Semiconductor Science (Proceedings of Rochester Conference, 1958) H. Brooks, Ed., Pergamon Press (1959).

(38) Scanlon, W. W., Solid State Physics, 9, 83 (1959).

(39) Kirglin, Elliott, and Cuff, Phys. Rev. Letters, 6, 177 (1961).

(40) Goldsmid, H. J., Proc. Royal Soc. (London), 71, 633 (1958), and 72, 17 (1958).

(41) Drabble, J. R., Advances in Semiconductor Science, Pergamon Press (1959).

(42) Ure, R. W., Jr., Bowers, R., and Miller, R. C., p 245, Properties of Elemental and Compound Semiconductors, H. C. Gatos, Ed., Interscience Publishers, N. Y., London (1960).

(43) Fischler, A. S., Phys. Rev., 122, 425 (1961).

(44) Soule, D. E., and McClure, J. W., J. Phys. Chem. Solids, 8, 29 (1959).

(45) Klein, C. A., and Holland, M. G., Phys. Rev., 136, A575 (1964).

EPS/LKM/BGK/RS/EHL:eh